1-1-2015

Combination Of Photodynamic Therapy With Fenretinide And C6-Pyridinium Ceramide Enhances Killing Of Scc17b Human Head And Neck Squamous Cell Carcinoma Cells Via The De Novo Sphingolipid Biosynthesis And Mitochondrial Apoptosis

Nithin Bhargava Boppana
Wayne State University,

COMBINATION OF PHOTODYNAMIC THERAPY WITH FENRETINIDE AND C6-PYRIDINIUM CERAMIDE ENHANCES KILLING OF SCC17B HUMAN HEAD AND NECK SQUAMOUS CELL CARCINOMA CELLS VIA THE *DE NOVO* SPHINGOLIPID BIOSYNTHESIS AND MITOCHONDRIAL APOPTOSIS

by

NITHIN BHARGAVA BOPPANA

THESIS

Submitted to the Graduate School

of Wayne State University,

Detroit, Michigan

in partial fulfillment of the requirements

for the degree of

MASTER OF SCIENCE

2015

MAJOR: PHARMACEUTICAL SCIENCES

Approved By:

_____

Advisor Date

DEDICATION

Dedicated to my mom Rekha Vasireddy for always believing in me and helping me in becoming the person who I am today.

ACKNOWLEDGEMENTS

I am grateful to my advisor, Dr. Duska Separovic for her invaluable mentorship throughout the project. Her input over this period helped me in developing personally and professionally. I am indebted to her as she constantly pointed out my mistakes and helped me to overcome them. I learned a lot of new things working with her, which I hope to utilize this knowledge in my future endeavors. I am very grateful to Dr. George Corcoran for believing in me and encouraging throughout my studies. I would next like to express gratitude for my committee members Dr. Timothy Stemmler, Dr. Fei Chen and Dr. Paul Stemmer in providing their invaluable time and feedback. I would like to acknowledge Dr. Mohamed Kodiha and Dr. Ursula Stochaj (Department of Physiology, McGill University, Montreal, Canada) for quantification of confocal microscopy images and for running statistical analysis for the quantification values. Additionally, I would like to thank Lipidomics Core (Medical University of South Carolina, Charleston, SC, USA) for running Mass Spectrometry. I would like to give many thanks to my colleagues Paul Breen, Nick Joseph, Younan Ma, John Boyd, and Jeremy DeLor for helping me through certain stages of the project. I am also grateful to my friends Sweeya, Avinash, Amit, Bhargav, Dileep and my other roommates for their encouragement and helping me through some difficult times. I am indebted to my mom and family members for always believing in me to achieve greater things and for their unwavering support at all times.

TABLE OF CONTENTS

LIST OF TABLES

LIST OF FIGURES

LIST OF ABBREVIATIONS

ABT	ABT-199
BSA	Bovine Serum Albumin
Cer	Ceramide
Cyt c	Cytochrome c
CERS	Ceramide synthase
DAPI	4'6-diamidino-2-phenylindole
DES	Dihydroceramide desaturase
DHCer	Dihydroceramide
DMEM	Dulbecco's Modified Eagle's Medium
ER	Endoplasmic reticulum
FB	Fumonisin B1
FBS	Fetal Bovine Serum
h	Hour/s
HNSCC	Head and Neck Squamous Cell Carcinoma
4HPR	N-(4-Hydroxyphenyl)retinamide
LCL29	C6-pyridinium ceramide
LD	Lethal dose
LSM	Laser scanning microscopy
MCRM	Mitochondrial ceramide-rich macrodomains
min	Minute/s
MS	Mass Spectrometry
PBS	Phosphate-buffered saline
PDT	Photodynamic therapy
Pc4	Phthalocyanine 4
RIPA	Radioimmunoprecipitation assay

ROS	Reactive oxygen species
rpm	Revolutions per minute
Sec	Second/s
SEM	Standard error of the mean
SL	Sphingolipid
zVAD	zVAD-fmk

CHAPTER 1: INTRODUCTION

1.1 Photodynamic therapy (PDT)

Photodynamic therapy is a cancer treatment modality. It is primarily used in treating pre-malignant and early stage cancers [1]. PDT involves three major components: a photosensitizer, light source, and tissue oxygen. Photosensitizers are sensitizing agents which are activated upon exposure to light of particular wavelength corresponding to their absorption spectrum. Photofrin, Foscan and Aminolevulinic acid are some of the currently available photosensitizers [2]. Lasers (argon dye, diode) and light-emitting diodes are used as light sources for PDT [3, 4].

Mechanism of PDT

Upon absorption of light, photosensitizer reaches its excited state. Two types of reactions can occur at this point. The excited photosensitizer can directly react with substrates like cell membrane to form radicals. Radicals then interact with oxygen to produce oxygenated products. This is known as a type I reaction. Alternatively, energy from the excited photosensitizer is directly transferred to oxygen thus forming singlet oxygen. This is known as a type II reaction [5]. Extent of the photodamage and cytotoxicity depends upon many factors such as the type and localization of photosensitizer, total dose of PDT, oxygen availability and time between administration of the photosensitizer and light exposure. PDT causes tumor destruction through direct tumor cell killing, vascular damage and activation of immune response [6].

PDT and apoptosis:

Apoptosis is shown with PDT in various cell lines [7-9]. Our previous studies have shown effect of modulation of *de novo* sphingolipid biosynthesis and ceramide synthases in PDT-induced apoptosis [10-12]. Studies have shown that PDT damages anti-apoptotic protein Bcl2 [13-15]. PDT was shown to induce Bax associated with mitochondria and cytochrome c release [9, 16-19].

1.2 C6-pyridinium ceramide (LCL29):

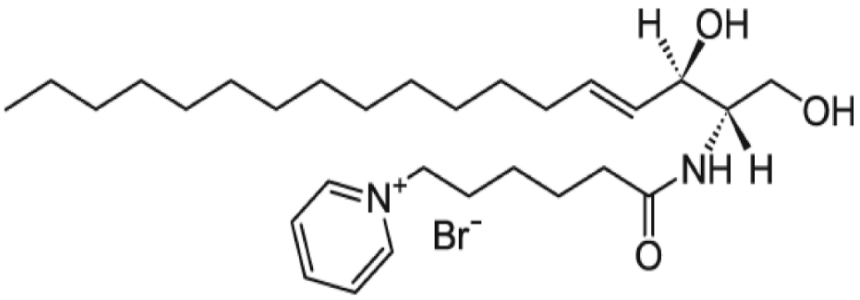

Figure 1.1 LCL29 structure (Courtesy of Avanti Polar Lipids)

LCL29 is a cationic water soluble C6-ceramide analog. Fixed positive charge allows targeting and delivery of LCL29 in to negatively charged mitochondria [20, 21]. LCL29 promotes Bax translocation to mitochondria leading to induction of mitochondrial membrane permeabilization and subsequent release of cytochrome c in to cytosol [22]. LCL29 in combination with PDT led to enhanced tumor cures [23, 24].

1.3 FENRETINIDE (4HPR):

4HPR is a synthetic retinoic acid derivative used for the treatment of cancer. 4HPR has been shown to be effective for treatment of breast cancer [25] and oral leukoplakia [26].

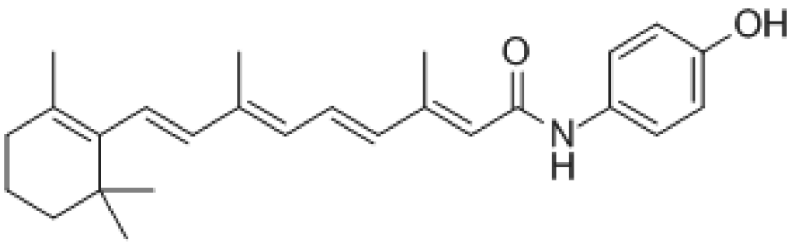

Figure 1.2 Structure of 4HPR (Courtesy of MedChem Express)

4HPR induces apoptosis in human head and neck squamous cell carcinoma (HNSCC), ovarian carcinoma and neuroblastoma cell lines [27-30]. Mechanism of apoptosis induction by 4HPR is not fully understood. Induction of Bax associated with mitochondria and cytochrome c release has been shown after 4HPR [9, 16-19].

1.4 Apoptosis

Apoptosis is a form of programmed cell death. Apoptosis is distinguished in to intrinsic and extrinsic apoptosis. Mitochondrial accumulation of Bax and cytochrome c (cyt c) release/redistribution are characteristics of mitochondrial or intrinsic apoptotic pathway [31]. Bax is a pro-apoptotic protein residing in cytosol, but translocates to mitochondria upon stress. Cytochrome c released in to the cytosol forms apoptosome by combining with Apaf-1 and procaspase-9 to activate caspase-9 which in turn activates caspase-3. Downstream targets are cleaved by active caspase-3 leading to apoptosis. Bcl2, an anti-apoptotic protein, has been shown to inhibit apoptosis by inhibiting Bax [32]. Pharmacological inhibitors can be used to test the role of apoptosis in stress-induced cell death. zVAD-fmk (zVAD) is a cell-permeable pancaspase inhibitor which irreversibly binds to caspase proteases at the catalytic site and inhibits induction of apoptosis [33]. ABT-199 (ABT) is a selective inhibitor of Bcl2 [34].

1.5 *De novo* sphingolipid biosynthesis

Ceramide can be generated in endoplasmic reticulum (ER) through the *de novo* sphingolipid (SL) biosynthesis pathway [35]. The *de novo* SL pathway involves ceramide synthase (CERS)-mediated conversion of dihydrosphingosine in to dihydroceramide by addition of a fatty acyl group. In the next step, dihydroceramide is further converted to ceramide by dihydroceramide desaturase-dependent reaction. Fumonisin B1 (FB) is an inhibitor of ceramide synthase [36, 37]. Fenretinide causes inhibition of dihydroceramide desaturase.

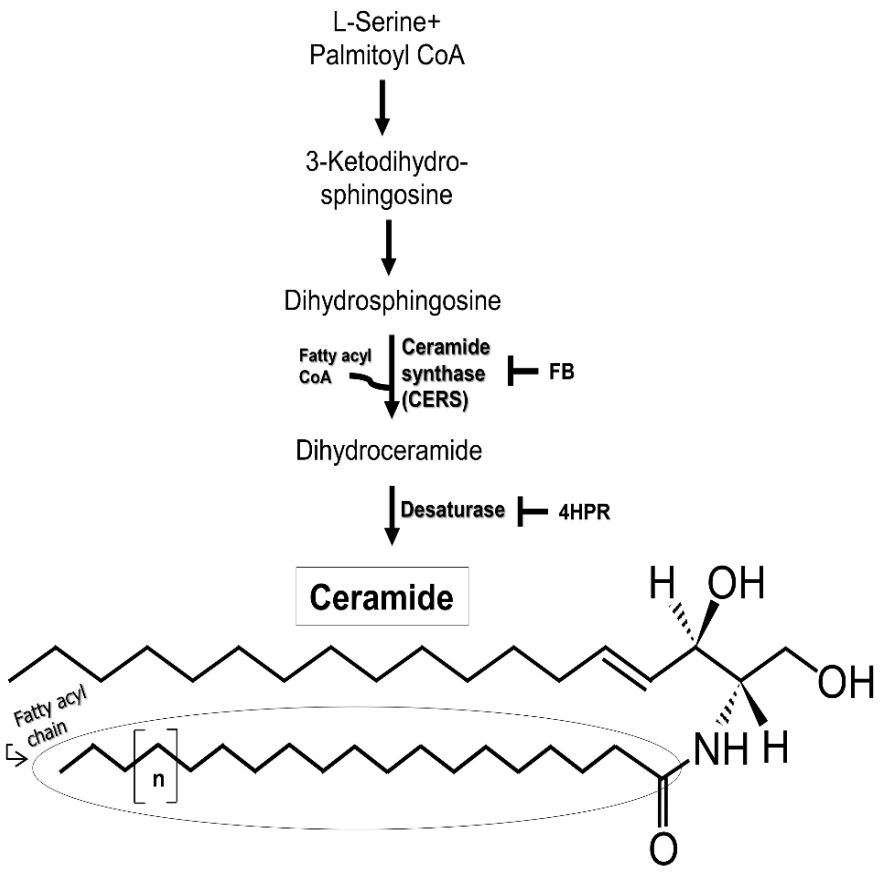

Figure 1.3 *De novo* sphingolipid biosynthesis pathway

1.6. Hypothesis

The hypothesis is that cell killing after PDT, PDT+4HPR and PDT+LCL29 is mediated via the *de novo* sphingolipid biosynthesis and mitochondrial apoptosis

CHAPTER 2: MATERIALS AND METHODS

2.1 Materials

Pc4 [$HOSiPcOSi(CH_3)_2(CH_2)_3N(CH_3)_2$], a silicon phthalocyanine photosensitizer was graciously provided by Dr. Malcolm E. Kenney (Case Western Reserve University, Cleveland, OH, USA). LCL29 [d-erythro-2-N-(6'-1"-pyridinium-hexanoyl sphingosine bromide)] was purchased from Avanti Polar Lipids (Alabaster, AL, USA). 4HPR [N-(4-Hydroxyphenyl) retinamide] was obtained from Sigma-Aldrich (St. Louis, MO, USA). Inhibitors were obtained from the following suppliers: Fumonisin B1 (Cayman Chemicals, Ann Arbor, MI, USA), zVAD-fmk (MBL International Corporation, Woburn, MA, USA) and ABT-199 (Selleck Chemicals, Houston, Texas, USA). DMEM/F-12 medium was purchased from Thermo-Fisher Scientific (Waltham, MA, USA). Fetal bovine serum (FBS) and goat serum were obtained from Sigma-Aldrich. Phosphate-buffered saline (PBS) without calcium and magnesium used for confocal microscopy was purchased from Life Technologies (Carlsbad, CA, USA). Phosphate-buffered saline with calcium and magnesium used for mass spectrometry and DEVDase assay was also purchased from Life Technologies.

2.2 Cell culture

SCC17B, a human head and neck squamous cell carcinoma cell line derived from larynx was supplied by Dr. Thomas Carey (University of Michigan, Ann Arbor, MI, USA). Cells were grown in DMEM/F-12 medium containing 10% fetal bovine serum, 100 units/ml penicillin, and 100 μg/ml streptomycin (Life Technologies) in a humidified incubator at 37°C and 5% CO_2. For all experiments, unless indicated otherwise, incubation of cells was carried out in a humidified incubator at 37°C and 5% CO_2. All treatments, as well as staining with Mitotracker Red CMXRos (see below) were added to cells in growth medium.

2.3 Treatments

After overnight (20 h) incubation with Pc4 (20 nM), LCL29 (1 μM) and 4HPR (2.5 μM) were added immediately prior to irradiation. Cells were irradiated at room temperature with red light (2 mW/cm^2; λ_{max} ~ 670 nm) using a light-emitting diode array light source (EFOS, Mississauga, ON, Canada) at the fluence of 200 mJ/cm^2. The inhibitors FB, zVAD (10 μM each) and ABT (0.1 μM) were added 1 h prior to treatments.

2.4 Clonogenic assay

In order to determine cell survival after treatments, clonogenic assay was employed to study the effect of treatments on colony formation ability of the cells. Modified pre-plating method was used as described previously in [38]. Cells were resuspended in growth medium with or without Pc4 and seeded (250 cells/well) in to 6-well plates (Thermo-Fisher Scientific). After overnight (20 h) incubation, the cells were irradiated. LCL29, 4HPR were added immediately prior to irradiation. The inhibitors FB, zVAD and ABT were added 1 h prior to treatments. After 14 days of incubation, the medium was aspirated, the plates were stained with crystal violet (0.1% in 20% ethanol; Sigma-Aldrich) for 30 seconds, rinsed with water and air-dried. Colonies (≥50 cells) were counted using eCount Colony Counter (VWR International, Radnor, PA, USA). Plating efficiency was 36% (n = 16).

2.5 Quantitative Confocal Microscopy

Ceramide/dihydroceramide accumulation in mitochondria and both ER, and Bax associated with mitochondria and cytochrome c redistribution were visualized using immunofluorescence and confocal microscopy. Immunofluorescence uses fluorescent-labeled antibodies for detection of specific target antigens. Fluorescent-labeled antibodies bind (directly or indirectly) to the antigen of interest, which allows for antigen detection using confocal microscopy. Sample preparation procedure for confocal microscopy is outlined below. Images were acquired using Zeiss LSM780 confocal microscope equipped with a 100 x 1.4 NA OIL DIC D objective (Carl Zeiss, Thornwood, NY, USA). Confocal microscopy imaging for all

experiments was performed at Microscopy, Imaging and Cytometry Resources Core, School of Medicine, Wayne State University (Detroit, MI, USA).

Outline of Immunofluorescence procedure for Confocal Microscopy visualization

Coverslips coated with Poly-L-Lysine and dried overnight

↓

Cell setup in 6-well plates containing cover slips

↓

Treatment of the samples and incubation for indicated period of time

↓

Addition of 250 nM Mitotracker Red CMXRos to the medium containing treated cells (For detection of mitochondria)

↓

Incubation for 30 min

↓

Medium aspirated and coverslips washed 3 times with coldPBS

↓

Cell fixation by incubation with 4% formalin (in PBS) for 15 min

↓

Formalin aspirated and coverslips washed 3 times with coldPBS

↓

Cell permeabilization by incubation with -20^{0}C Acetone/Methanol (1:1) for 10 min

↓

Acetone/Methanol aspirated and coverslips washed 3 times with coldPBS

↓

Addition of 3% Goat Serum+ 3% FBS in PBS to wells and incubation for 1 h at 4^{0}C

↓

Serum aspirated and coverslips washed 3 times with coldPBS

↓

Incubation of coverslips with primary antibodies (diluted in 1% BSA, 0.025% Tween 20 in PBS solution) at room temperature for 45 min

↓

Coverslips washed 3 times with coldPBS

↓

Incubation of coverslips with fluorophore-conjugated secondary antibodies (diluted in 1% bovine serum albumin, 0.025% Tween 20 in PBS solution) at room temperature for 45 min

↓

Coverslips washed 3 times with coldPBS

↓

Incubation of coverslips with DAPI (1 µg/ml in PBS; Life Technologies) for 10 min at room temperature

↓

Coverslips washed 3 times with coldPBS

↓

Coverslips mounted on to slides using Antifade kit

↓

Visualization with confocal microscopy

Table 2.1 Primary antibodies used in quantitative confocal microscopy

Primary antibody	**Target**	**Vendor**
Anti-ceramide/dihydroceramide antibody	Ceramide, Dihydroceramide	Enzo Life Sciences
Anti-KDEL antibody	Endoplasmic reticulum	Abcam
Anti-Bax antibody	Bax	Abcam
Anti-cyt c antibody	Cytochrome c	BD Pharmingen

Table 2.2 Secondary antibodies used in quantitative confocal microscopy

Secondary antibody	Target (Primary antibody)	Vendor
Alexa 488-conjugated Goat anti-mouse IgM antibody	Anti-ceramide/ dihydroceramide antibody	Jackson-Immunoresearch
Alexa 594-conjugated Goat anti-mouse IgG antibody	Anti-KDEL and anti-cyt c antibodies	Jackson-Immunoresearch
Alexa 488-conjugated Goat anti-mouse IgG antibody	Anti-Bax antibody	Jackson-Immunoresearch

2.6 Quantification of Confocal Microscopy Images

Ceramide/dihydroceramide fluorescence associated with the ER and the mitochondria, as well as Bax fluorescence associated with the mitochondria were quantified by Dr. Ursula Stochaj and Dr. Mohamed Kodiha, Department of Physiology, McGill University, Montreal, Canada. MetaXpress software version 5 5.00.20 (Molecular Devices, Sunnyvale, CA, USA) was used for the quantification [39]. Mitotracker CMXRos (Life Technologies) or anti-KDEL antibodies were used to demarcate the mitochondria or the ER. Visual inspection was used to verify identification of correct compartments. Multiwavelength cell scoring module was employed in measuring ceramide/dihydroceramide pixel intensities associated with mitochondria and ER and Bax pixel intensities associated with mitochondria. Prior to quantification, all the images were corrected for background contribution. Cytochrome c redistribution was quantified using visual inspection of the confocal microscopy images. Margin of cytochrome c staining greater than 10 μm around the nuclei was used as a criteria for scoring cells positive for cytochrome c redistribution. In all experiments, atleast 100 cells were assessed for each condition.

2.7 Mass Spectrometry (MS)

Mass spectrometry was used to determine effect of treatments on different sphingolipids. Ten hours after treatments, cells were collected on ice and centrifuged at 750 g for 10 min at 4^0C in Allegra 6KR centrifuge (Beckman Coulter, Pasadena, CA, USA). After aspirating the

supernatants, cell pellets were resuspended in cold PBS. An aliquot of the sample was transferred to a different tube for determining protein content. Remaining sample was centrifuged at 325 g for 5 min at 4^0C in Allegra 6KR centrifuge. Supernatant was aspirated and cell pellet was resuspended in 1:1 mixture of methanol and ethyl acetate (EMD chemicals, Billercia, MA, USA). Samples were then dried under nitrogen and shipped overnight on dry ice to the Lipidomics shared resource facility located in Medical University of South Carolina (Charleston, SC, USA) for further processing. After extraction, sphingolipids were separated by high performance liquid chromatography and analyzed using TSQ 7000 triple quadrupole mass spectrometer (Thermo-Fisher Scientific) [40]. After determining protein content, pmoles of sphingolipids were normalized per mg protein and data were expressed as average ± SEM (n=3-4).

2.8 DEVDase activity assay

DEVDase assay was used for measuring caspase-3 activity in the cytosol as described previously [41]. This assay is based upon quantitative measurement of enzyme's cleavage of a fluorogenic substrate N-acetyl-Asp-Glu-Val-Asp (DEVD; Enzo life sciences, Ann Arbor, MI, USA). Briefly, 24 h after treatments, cells were collected on ice and centrifuged at 750 g for 10 min at 4^0C in Allegra 6KR centrifuge (Beckman Coulter). After aspirating the supernatants, cell pellets were resuspended in phosphate-buffered saline (Life Technologies). Resuspension was followed by centrifugation at 1650 g for 5 min at 4^0C in Sorvall Fresco microcentrifuge (Thermo-Fisher Scientific). After aspirating the supernatants, cell pellets were resuspended in RIPA (Radioimmunoprecipitation assay) lysis buffer (VWR international) and vortexed thoroughly. Samples were then centrifuged at 6500 g for 10 min at 4^0C in Sorvall Fresco microcentrifuge and supernatants were collected. Protein content of the samples was determined. Volume containing 25 µg protein/sample was added to assay buffer and DEVD substrate, incubated for 1 h at 37^0C in a water bath. Spectroflourometer (F-2500 Hitachi, New York, NY, USA; 380 nm excitation and 460 nm emission) was then used to measure the fluorescence of the cleaved

DEVD substrate. Assay buffer added to DEVD substrate without the sample was used as a blank. Blank value was subtracted from the treatments to get caspase-3 activity in arbitrary units.

2.9 Protein determination

Protein content was determined by a modified Bradford assay, based on the shift in absorption maximum (λ_{max}) of the protein assay dye (Bio-Rad, Hercules, CA, USA) upon binding to proteins. Concentration of the protein in the sample was calculated by measuring the absorbance at 595 nm, which was proportional to amount of dye bound to the protein. Briefly, this procedure involves serial dilution of the samples with double distilled water to avoid saturation of the dye. The protein assay dye was then added to the diluted samples and incubated for 30 min at room temperature. Double distilled water added to the dye without any sample is used as a blank. After incubation, a synergy microplate reader (BioTek, Winooski, VT, USA) was used to measure the absorbance at 595 nm. Blank value was subtracted from the absorbance of treatments and used for calculating protein content. A standard curve generated using bovine serum albumin was employed to determine the protein content in the samples.

2.10 Statistical analysis

Clonogenic, mass spectrometry and DEVDase data are presented as the average ± SEM. Significant differences ($p < 0.05$) in clonogenic, mass spectrometry and DEVDase values was determined using student's t-tests. One-way ANOVA was used to determine significant differences ($p < 0.05$) in confocal quantification data. Statistical analysis using one-way ANOVA were run by Dr. Ursula Stochaj (Department of Physiology, McGill University, Montreal, Canada).

CHAPTER 3: RESULTS AND DISCUSSION

3.1 PDT data:

PDT-induced cell death is inhibited by FB and zVAD and enhanced by ABT

Our previous studies have shown that PDT-induced apoptosis requires *de novo* SL synthesis and CERS in cell lines other than SCC17B cells [10-12]. However, it is not known whether the PDT-induced cell killing requires CERS. Bcl2 protects against PDT-induced cell killing in apoptosis-competent cells (e.g. human breast cancer MCF-7 cells overexpressing human pro-caspase 3) [42]. However, it has yet to be determined whether in SCC17B cells, apoptosis is essential for PDT-induced killing. It is also not known whether inhibition of Bcl2 sensitizes these cells to PDT. To define the requirement for CERS, caspases, and Bcl2 in PDT-induced cell killing, different pharmacological inhibitors were employed: the CERS inhibitor FB, the pan-caspase inhibitor zVAD, and the Bcl2 inhibitor ABT. All inhibitors FB, zVAD and ABT were used at non-toxic doses. PDT was used at LD20 (20 nM Pc4+ 200 mJ/cm^2), as determined in dose-response studies (not shown). As shown in figure 3.1, FB and zVAD-inhibited cell killing after PDT by 68 and 56%, respectively. ABT enhanced PDT-induced cell killing by 61% (Fig 3.1). Together, the data indicate that PDT-induced cell killing depends on CERS, caspase activation, and Bcl2.

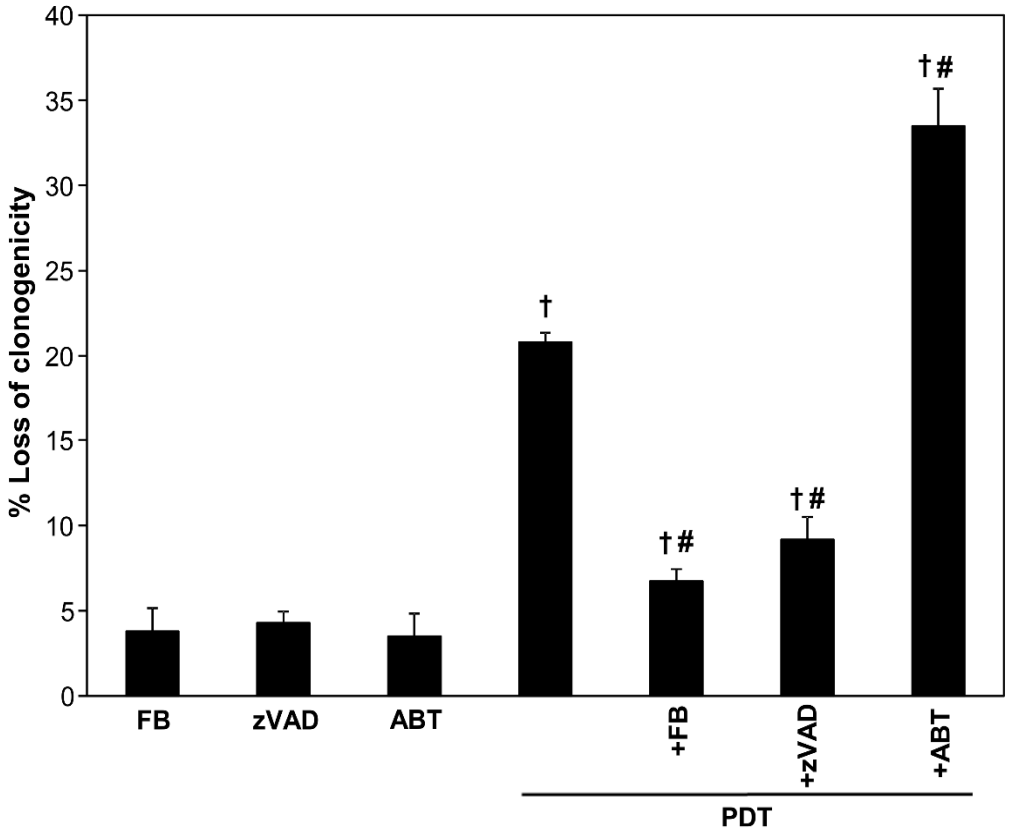

Figure 3.1 PDT-induced cell killing is sensitive to FB, zVAD and ABT. FB, zVAD (10 μM each) and ABT (0.1 μM) were added 1 h prior to PDT (20 nM Pc4+200 mJ/cm^2). Colonies were stained with crystal violet (0.1%) and counted 14 days after treatments. The data are shown as the average ± SEM (n = 6-18). Significant differences are shown between: **†**, treatment and untreated control; **#**, (treatment + inhibitor) and treatment. Untreated controls had 0% loss of clonogenicity (Taken from Photochem. Photobiol. 13, 1621-27, 2014).

PDT-induced ceramide/dihydroceramide accumulation in the ER and mitochondria is inhibited by FB

The subcellular localization of ceramide correlates with the specificity of its biological effects. CERS-dependent ceramide accumulation has been associated with ER stress and apoptosis [43]. On the other hand, FB-sensitive mitochondrial ceramide accumulation has been linked to radiation-induced apoptosis [44]. We have previously shown that PDT-induced ceramide accumulation involves the *de novo* SL biosynthesis and CERS [10-12], which implies generation of ceramide in the ER. However, experimental evidence for PDT-induced ceramide

accumulation in the ER is missing. Also, evidence that PDT induces mitochondrial ceramide accumulation is lacking.

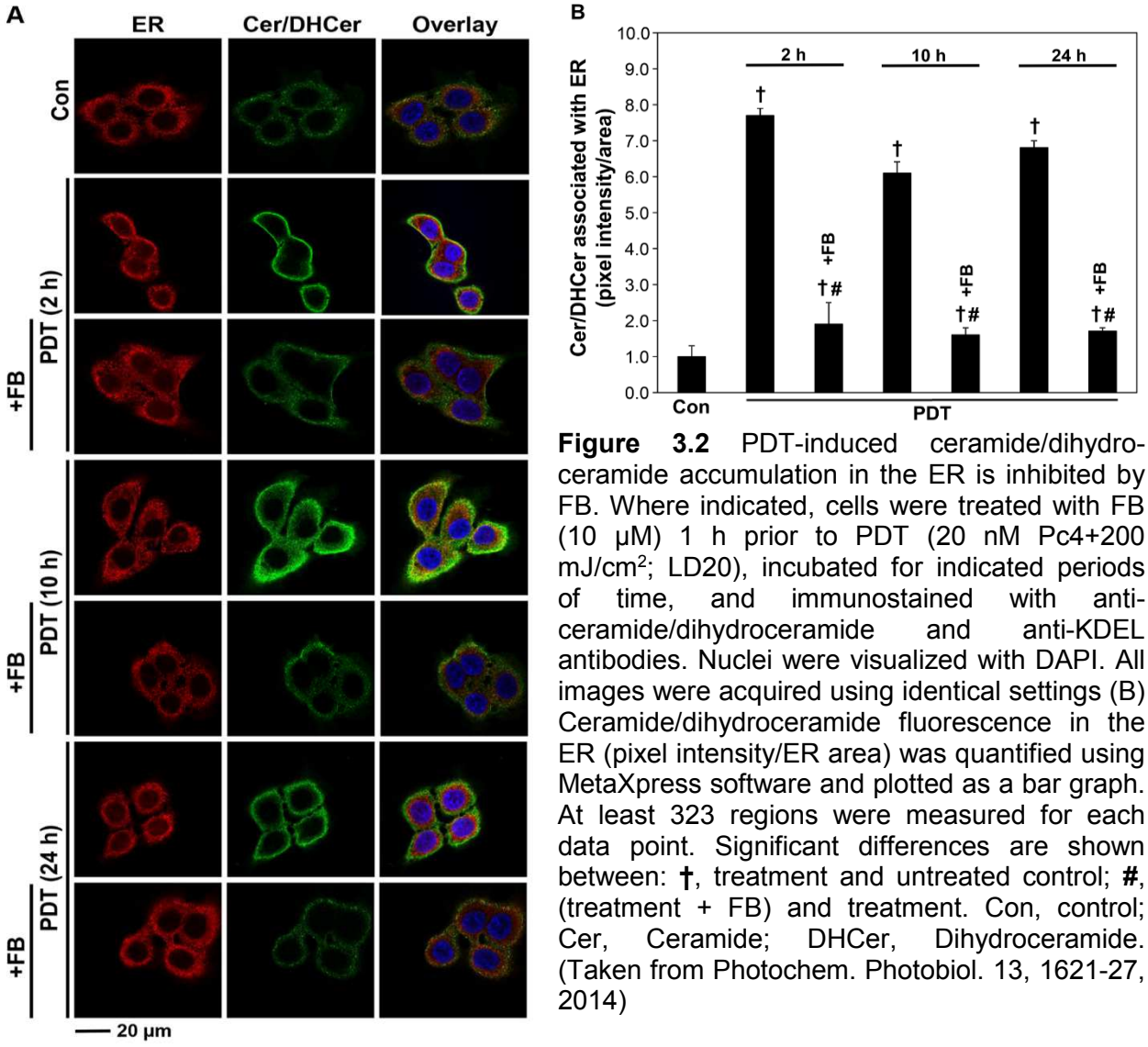

Figure 3.2 PDT-induced ceramide/dihydroceramide accumulation in the ER is inhibited by FB. Where indicated, cells were treated with FB (10 µM) 1 h prior to PDT (20 nM Pc4+200 mJ/cm^2; LD20), incubated for indicated periods of time, and immunostained with anti-ceramide/dihydroceramide and anti-KDEL antibodies. Nuclei were visualized with DAPI. All images were acquired using identical settings (B) Ceramide/dihydroceramide fluorescence in the ER (pixel intensity/ER area) was quantified using MetaXpress software and plotted as a bar graph. At least 323 regions were measured for each data point. Significant differences are shown between: **†**, treatment and untreated control; **#**, (treatment + FB) and treatment. Con, control; Cer, Ceramide; DHCer, Dihydroceramide. (Taken from Photochem. Photobiol. 13, 1621-27, 2014)

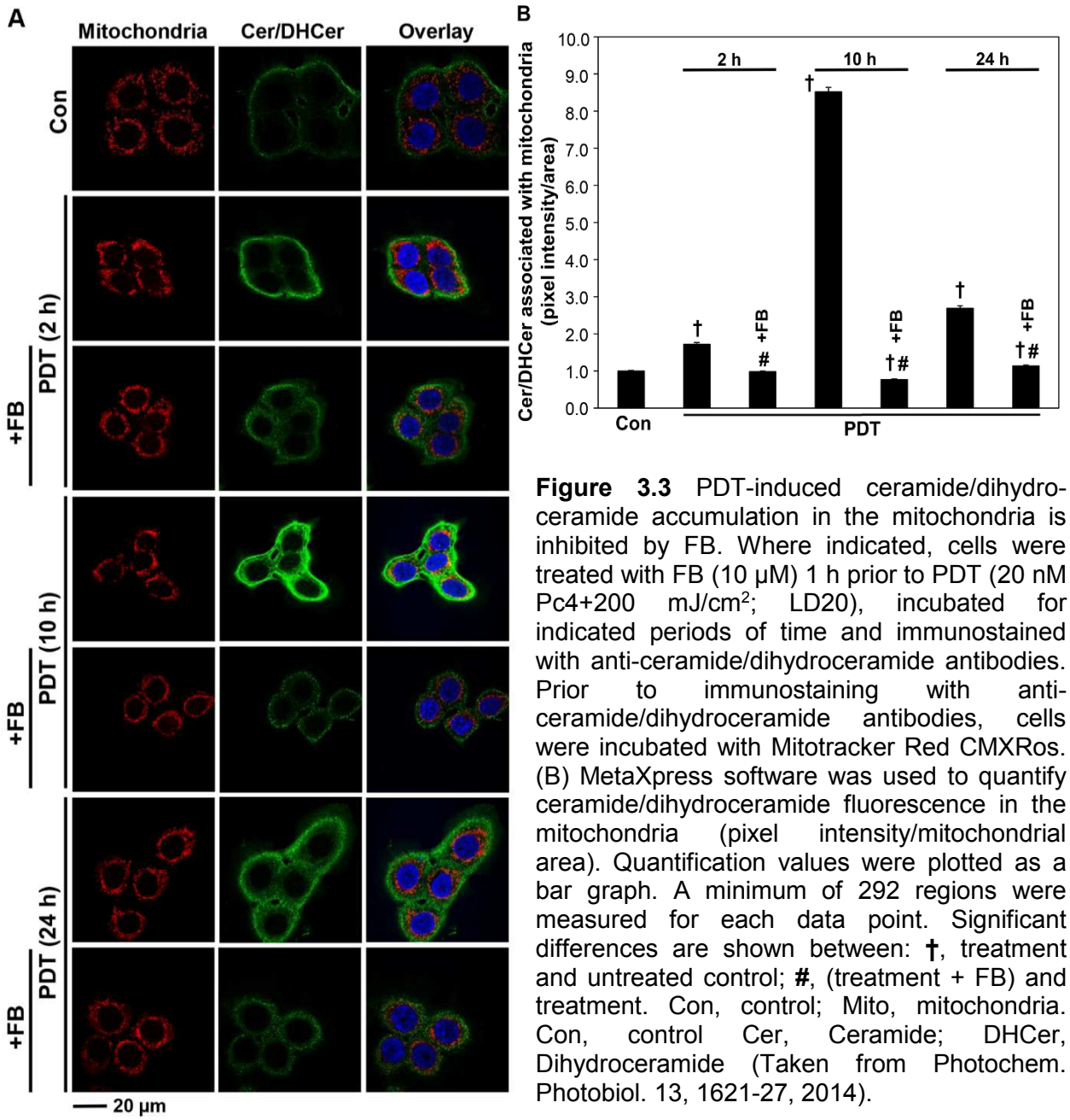

Figure 3.3 PDT-induced ceramide/dihydroceramide accumulation in the mitochondria is inhibited by FB. Where indicated, cells were treated with FB (10 µM) 1 h prior to PDT (20 nM Pc4+200 mJ/cm^2; LD20), incubated for indicated periods of time and immunostained with anti-ceramide/dihydroceramide antibodies. Prior to immunostaining with anti-ceramide/dihydroceramide antibodies, cells were incubated with Mitotracker Red CMXRos. (B) MetaXpress software was used to quantify ceramide/dihydroceramide fluorescence in the mitochondria (pixel intensity/mitochondrial area). Quantification values were plotted as a bar graph. A minimum of 292 regions were measured for each data point. Significant differences are shown between: †, treatment and untreated control; #, (treatment + FB) and treatment. Con, control; Mito, mitochondria. Con, control Cer, Ceramide; DHCer, Dihydroceramide (Taken from Photochem. Photobiol. 13, 1621-27, 2014).

Here, we used for the first time quantitative confocal microscopy to measure ceramide/dihydroceramide in mitochondria and the ER. To this end, ceramide/dihydroceramide was detected by immunostaining; Mitotracker and KDEL served as markers of mitochondria and the ER, respectively. As depicted in Figures 3.2 and 3.3, we determined the accumulation of ceramide/dihydroceramide in the ER and mitochondria at 2, 10 and 24 h post-PDT.

Ceramide/dihydroceramide accumulation at both subcellular sites increased post-PDT, as quantification data revealed (Fig. 3.2.B and 3.3.B). Next we used FB to test whether PDT-induced ceramide/dihydroceramide accumulation is CERS-dependent. FB reduced ceramide/dihydroceramide accumulation in the ER and mitochondria post-PDT at all-time points [Fig. 3.2 and 3.3]. This was also confirmed by the quantification analysis (Fig. 3.2.B and 3.3.B). Together these results reveal that PDT induces ceramide/dihydroceramide accumulation in the ER and mitochondria. The data suggest that PDT-induced ceramide/dihydroceramide accumulation at ER and mitochondria is CERS-dependent.

MS reveals increases in ceramides post-PDT

To validate confocal microscopy findings, we used MS to identify ceramide species accumulated in response to PDT. The levels of most of the individual ceramides were significantly increased after PDT [Table 3.2]. PDT also increased the levels of C16-dihydroceramide, a precursor of ceramide in *de novo* SL biosynthesis. Overall, our data demonstrate increases in the levels of ceramides and C16-dihydroceramide post-PDT. They also suggest the involvement of the *de novo* SL biosynthesis.

PDT-induced Bax translocation to mitochondria and cyt c redistribution are inhibited by FB

The translocation of the pro-apoptotic protein Bax from the cytosol to mitochondria and the redistribution of cyt c from the mitochondria to the cytosol are hallmarks of the mitochondrial pathway of apoptosis and have been demonstrated in response to PDT [9, 15, 17, 45]. However, it is not known whether PDT induces Bax associated with mitochondria and cyt c redistribution in SCC17B cells. It is also not clear whether these processes are CERS-dependent. Using quantitative confocal microscopy, we determined whether Bax associated with mitochondria and cyt c redistribution are induced by PDT and sensitive to FB. As shown in Figure 3.4, Bax associated with mitochondria was induced at 2 and 10 h post-PDT. In the presence of FB, this process was inhibited. Cyt c redistribution was observed at 10 h post-PDT

[Fig. 3.5] but not earlier (not shown). Co-treatment of cells with FB and PDT led to inhibition of cyt c redistribution. Together, these results indicate that PDT induces Bax associated with mitochondria and cyt c redistribution in SCC17B cells. Moreover, both processes are CERS-dependent.

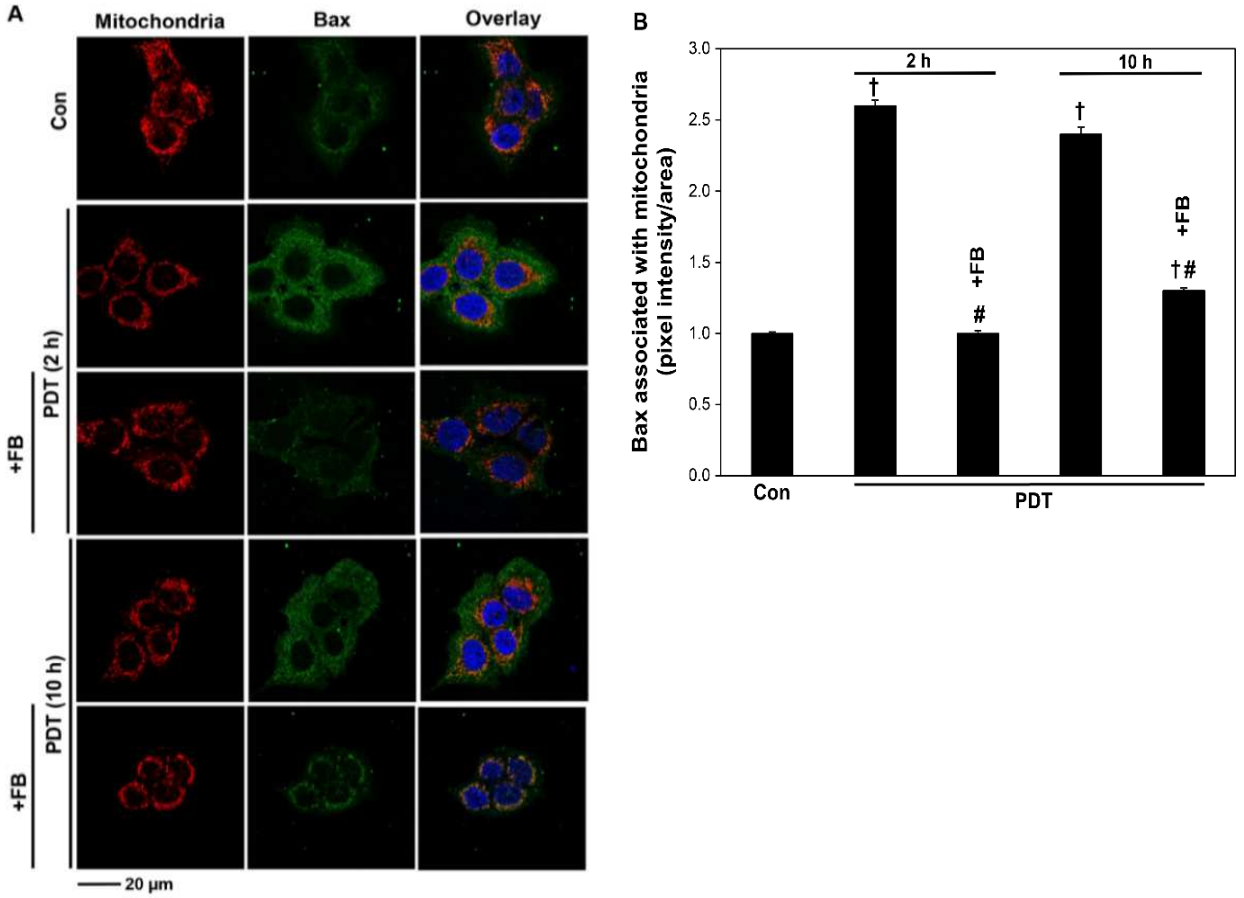

Figure 3.4 PDT-induced Bax associated with mitochondria is inhibited by FB. FB (10 µM) was added 1 h prior to PDT (20 nM Pc4+200 mJ/cm^2; LD20). Cells were incubated for indicated periods of time and then immunostained with anti-Bax antibodies. Incubation with Mitotracker Red CMXRos was carried out prior to immunostaining with anti-Bax antibodies. Images were acquired by confocal microscopy using identical settings. (B) Bax fluorescence associated with mitochondria was quantified using MetaXpress software. The data were calculated as Bax-pixel intensities/mitochondrial area. A minimum of 277 regions were measured for each data point. Results are shown as the average ±SEM. Significant differences are shown between: **†**, treatment and untreated control; **#**, (treatment + FB) and treatment. Con, untreated control (Taken from Photochem. Photobiol. 13, 1621-27, 2014)

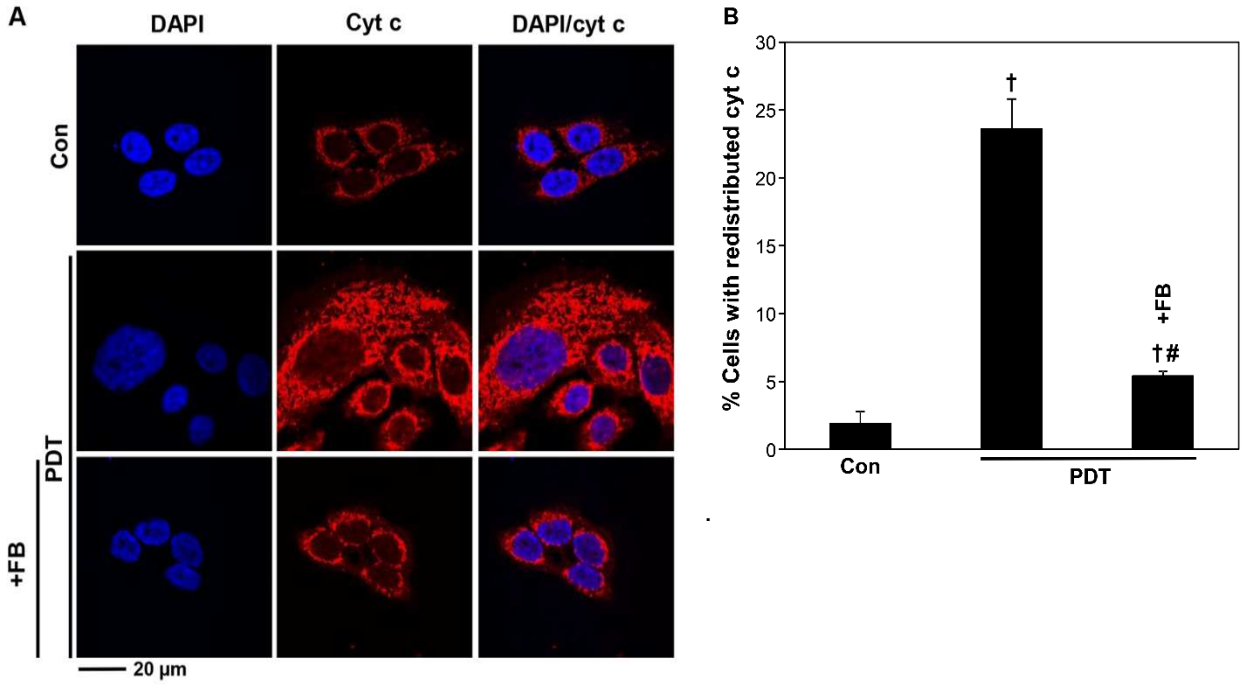

Figure 3.5 PDT-induced cytochrome c redistribution is inhibited by FB. FB (10 µM) was added 1 h prior to PDT (20 nM Pc4+200 mJ/cm^2; LD20). Cells were incubated for indicated periods of time and then immunostained with anti-cyt c antibodies. Images were acquired by confocal microscopy using identical settings. (B) Percentages of cells with cyt c redistribution were calculated by scoring 100 cells for every sample and were plotted as bar graph. Each data point represents 3-4 samples and the data are shown as the average ± SEM. Significant differences are shown between: **†**, treatment and untreated control; **#**, (treatment + FB) and treatment. Con, untreated control (Taken from Photochem. Photobiol. 13, 1621-27, 2014).

FB inhibits caspase-3 activation after PDT

DEVDase assay was used to test the activation of caspase-3 after PDT. As shown in figure 3.10, caspase-3 was activated at 24 h post-PDT. Co-treatment of cells with FB and PDT led to inhibition of caspase-3 activation.

Conclusion

The present studies demonstrate that inhibition of CERS and caspases protect cells from PDT-induced killing, indicating that PDT induces apoptotic cell killing in SCC17B cells via CERS. In addition, inhibition of Bcl2 enhances PDT-induced cell killing in these cells, which further supports the idea that apoptosis is involved. PDT-induced accumulation of ceramide/dihydroceramide in the ER and mitochondria is inhibited by FB. PDT-induced Bax

associated with mitochondria, and cytochrome c redistribution, are sensitive to FB. These findings highlight the functional significance of mitochondrial apoptosis and CERS in cell killing in response to PDT. In summary, these results suggest that CERS-dependent ceramide/dihydroceramide accumulation is required for apoptotic cell death after PDT.

3.2 PDT+4HPR data:

Enhanced cell killing after PDT+4HPR is FB-, zVAD- and ABT-sensitive

Clonogenic assay was used to test whether combining PDT with 4HPR sensitizes SCC17B cells to PDT. As shown in Table 3.1, when PDT and 4HPR were used at LD20 each, i.e. the dose reducing survival by 20%, 63% of PDT+4HPR-treated cells were unable to form colonies. To determine whether apoptosis and ceramide synthase are necessary for enhanced cell killing after PDT+4HPR, pancaspase inhibitor zVAD, the Bcl2 inhibitor ABT, and the ceramide synthase inhibitor FB were used. All inhibitors were non-toxic (LD < 5). FB and zVAD rendered the cells resistant not only to PDT and 4HPR alone, but also to PDT+4HPR. In contrast, ABT sensitized SCC17B cells to PDT±4HPR. This suggest that PDT+4HPR-induced enhanced cell killing of SCC17B cells depends on ceramide synthase, caspase activation and inhibition of Bcl2.

Table 3.1 PDT+4HPR-induced augmented cell killing is FB-, zVAD- and ABT-sensitive.

Treatment	% Survival
4HPR	80 ± 0.6[a]
4HPR+FB	91 ± 0.9[a,b]
4HPR+zVAD	95 ± 1.0[b]
4HPR+ABT	73 ± 0.7[a,b]
PDT	79 ± 0.6[a]
PDT+FB	93 ± 0.7[b]
PDT+zVAD	91 ± 1.3[a,b]
PDT+ABT	67 ± 2.2[a,b]
PDT+4HPR	37 ± 0.7[a,c]
PDT+4HPR+FB	73 ± 1.7[a,b]
PDT+4HPR+zVAD	91 ± 1.6[b]
PDT+4HPR+ABT	32 ± 0.9[a,b]

FB, zVAD (10 μM each) and ABT (0.1 μM) were added 1 h prior to PDT (20 nM Pc4+200 mJ/cm^2), 4HPR (2.5 μM) or the combination. Colonies were stained with crystal violet (0.1%) and counted 14 days after treatments. The data are shown as the average ± SEM (n = 3-18 samples). Significant differences are shown between: [a], treatment and untreated control; [b], (treatment + inhibitor) and treatment; [c], combination and individual treatments (Taken from Int. J. Oncol. 46, 2003-10, 2015).

PDT+4HPR enhances ceramide/dihydroceramide accumulation in the ER. FB inhibits ceramide/dihydroceramide accumulation in the ER and mitochondria after PDT±4HPR

Because the *de novo* SL biosynthesis pathway is localized to the ER, we tested the effect of combining PDT with 4HPR on dihydroceramide/ceramide accumulation in the ER. Using an antibody that recognizes dihydroceramide and ceramide [46] and the ER marker anti-KDEL for quantitative confocal microscopy, we found that PDT+4HPR enhanced dihydroceramide/ceramide accumulation in the ER (Fig. 3.6). This effect was inhibited by FB. It is unknown what impact on mitochondrial dihydroceramide/ceramide accumulation combining PDT with 4HPR might have. Using the same anti-dihydroceramide/ceramide antibody and the

mitochondrial marker Mitotracker for quantitative confocal microscopy, we found that PDT and 4HPR alone did induce mitochondrial dihydroceramide/ceramide accumulation (Fig. 3.6). However, the effect was not enhanced after PDT+4HPR. FB inhibited mitochondrial ceramide accumulation after all treatments.

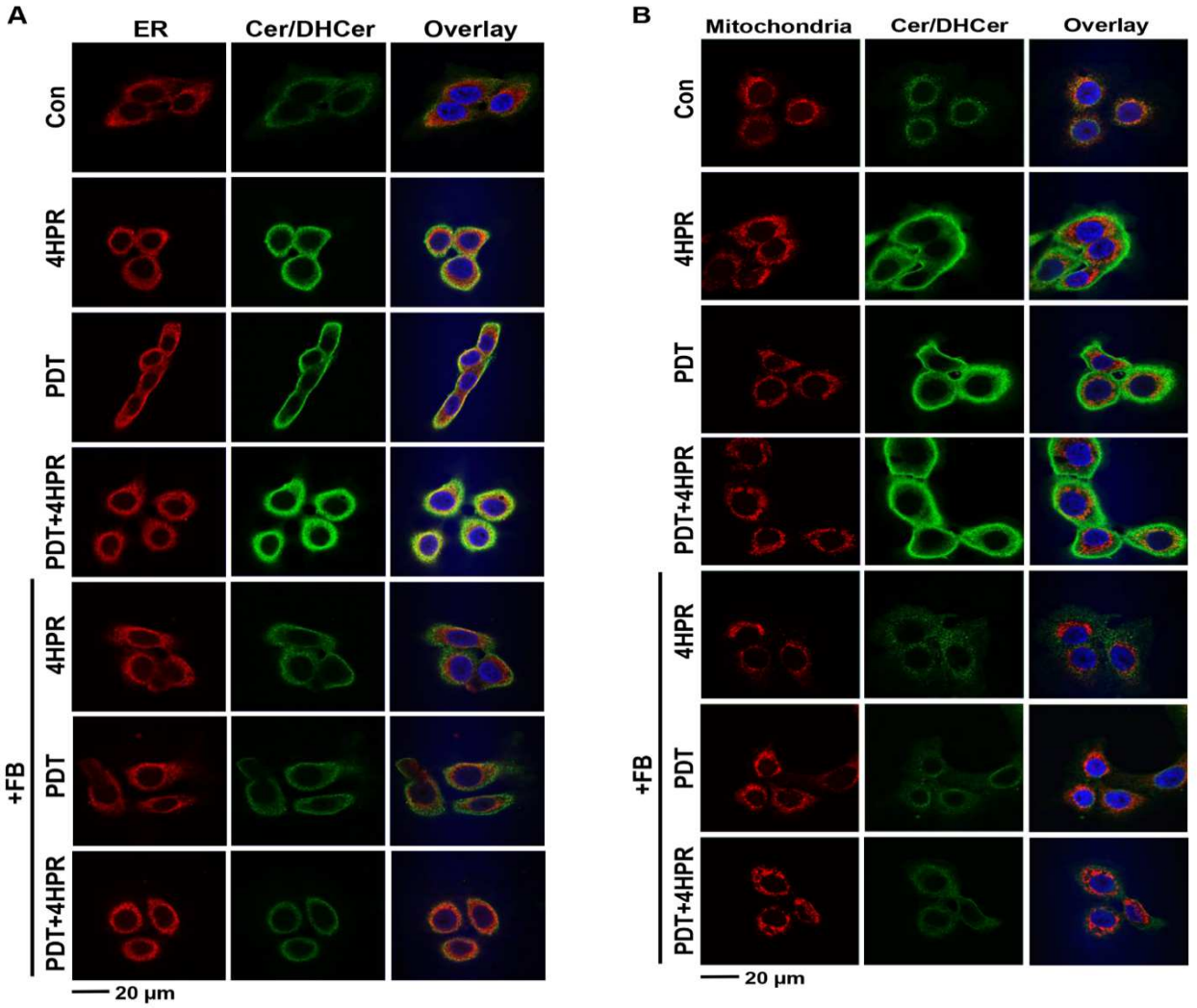

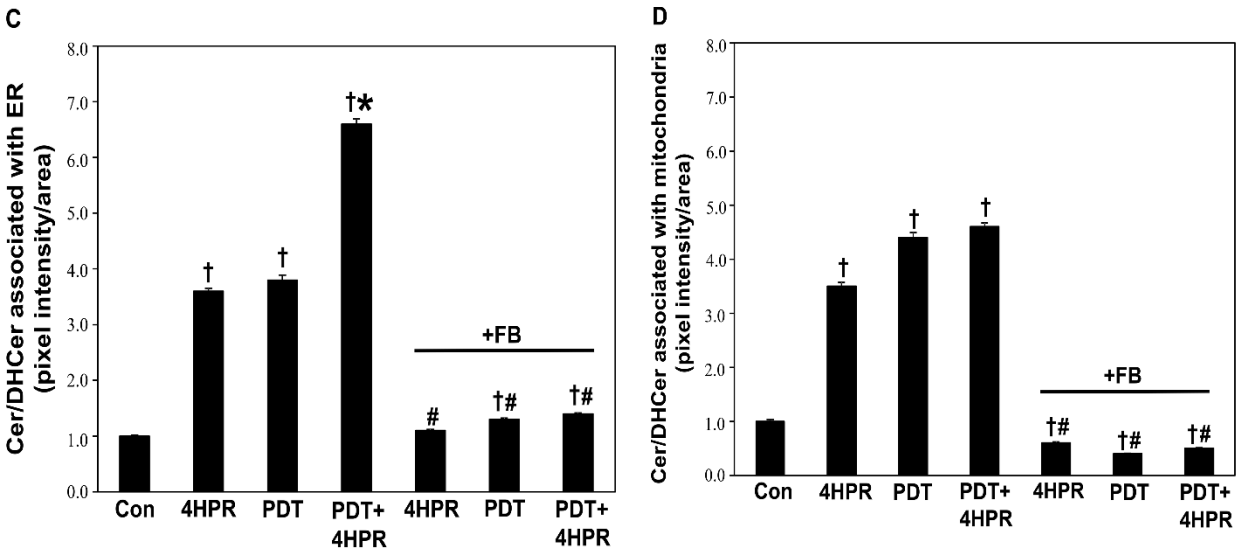

Figure 3.6 PDT+4HPR enhanced ceramide/dihydroceramide accumulation in the ER is inhibited by FB. FB inhibits ceramide/dihydroceramide accumulation in mitochondria after PDT±4HPR. Cells were treated with FB (10 μM) 1 h prior to PDT (20 nM Pc4+200 mJ/cm^2; LD20), 4HPR (2.5 μM; LD20), or the combination, incubated for 10 h, immunostained with anti-ceramide/dihydroceramide and, anti-KDEL antibodies (A, C). (B, D) Incubation with Mitotracker Red CMXRos was carried out prior to immunostaining with anti-ceramide antibodies. Nuclei were visualized with DAPI. All images were acquired by confocal microscopy with identical settings. MetaXpress software was used to quantify ceramide/dihydroceramide fluorescence located in the ER (B) and mitochondria (D). (B and D) Data are shown as the average ± SEM. The graphs depict ceramide/dihydroceramide fluorescence/ER area (B), or ceramide/dihydroceramide fluorescence/mitochondrial area (D). Results were normalized to the untreated control. Significant differences are shown between: **†**, treatment and untreated control; **#**, (treatment + FB) and treatment; ***,** combination and individual treatments. Con, control; Cer, Ceramide; DHCer, Dihydroceramide (Taken from Int. J. Oncol. 46, 2003-10, 2015).

PDT+4HPR enhances C16-dihydroceramide, not ceramide, accumulation

Both PDT and 4HPR regulate the *de novo* SL biosynthesis pathway [10, 41, 47, 48]. The question is what the effects of combining PDT with 4HPR on the cellular SL profile are. We used MS to address the question. As depicted in Figure 3.7.A, in contrast to 4HPR, PDT increased total ceramide accumulation. Combining PDT with 4HPR attenuated PDT-induced increase in total ceramide levels. The accumulation of individual ceramides, by and large, followed the same pattern (Table 3.2). 4HPR did not significantly raise the levels of any individual ceramide. In contrast, 4HPR increased accumulation of C16-dihydroceramide, a *de novo* SL biosynthesis pathway metabolite by 445% above basal levels (Fig. 3.7.B). PDT also increased the levels of C16-dihydroceramide by 138% beyond resting levels. Combining PDT with 4HPR enhanced accumulation of C16-dihydroceramide by 632%. These results show that PDT+4HPR led to increase in C16-dihydroceramide levels rather than individual and total ceramide levels.

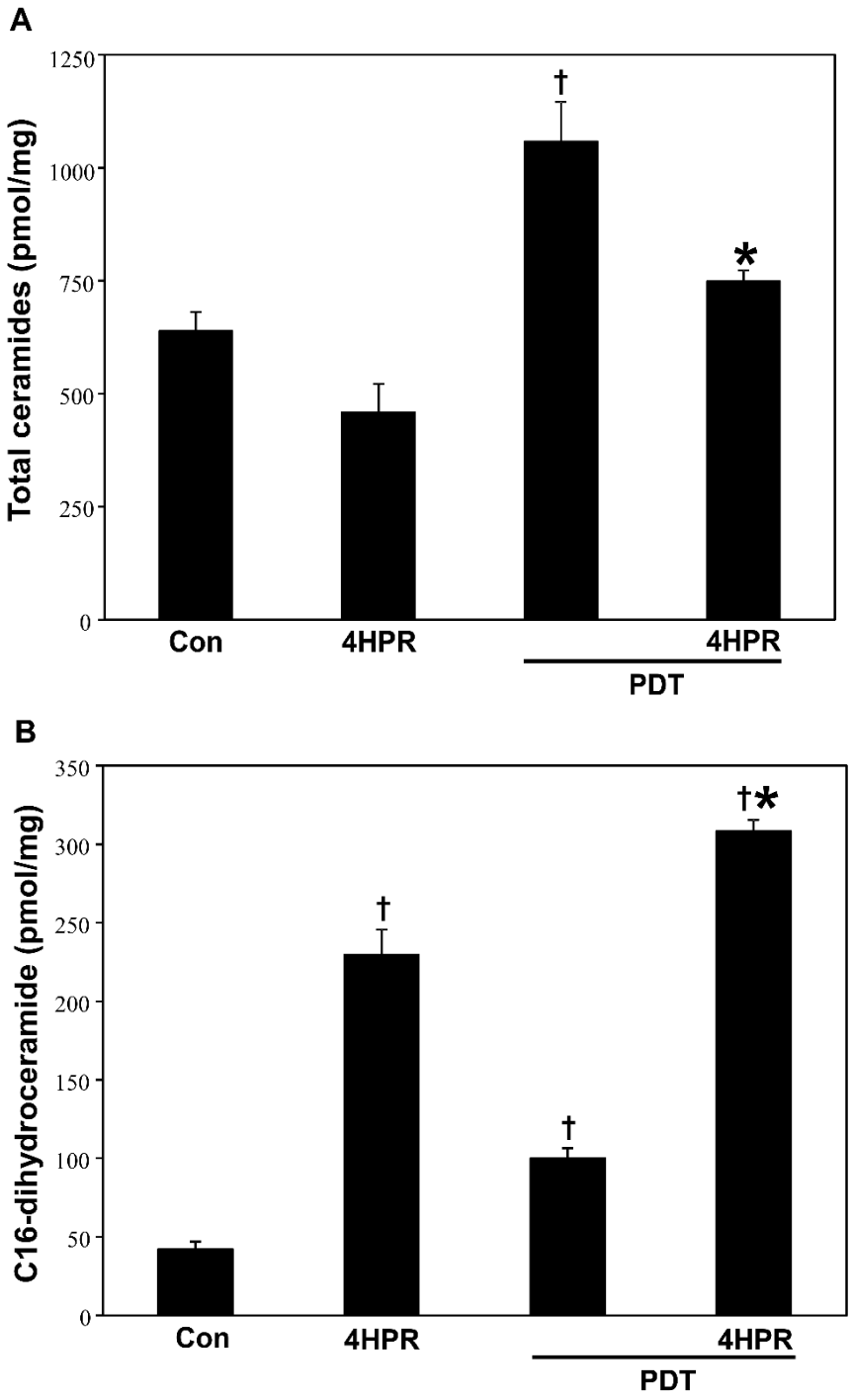

Figure 3.7 Effect of PDT+4HPR on total ceramide levels (A). PDT+4HPR enhances C16-dihydroceramide accumulation (B). Cells were treated with PDT (20 nM Pc4 + 200 mJ/cm^2; LD20), 4HPR (2.5 μM; LD20) or the combination, incubated for 10 h, collected and processed for MS. The levels of sphingolipids were calculated as pmoles/mg protein and are shown as the average ± SEM (n=3-4). Significant differences are shown between: **†**, treatment and untreated control; *****, combination and individual treatments. Con, untreated control (Taken from Int. J. Oncol. 46, 2003-10, 2015).

Table 3.2 Effect of PDT ± 4HPR on individual ceramides in SCC17B cells.

Ceramide	Con	4HPR	PDT	PDT+4HPR
C14-ceramide	16.1 ± 0.9	16.7 ± 1.8	29.4 ± 1.7[a]	22.6 ± 0.8[a,d]
C16-ceramide	91.0 ± 11.9	51.7 ± 6.4[a]	129.6 ± 8.5[a]	93.5 ± 3.6[d]
C18-ceramide	17.8 ± 2.1	21.5 ± 3.0	61.6 ± 4.2[a]	48.3 ± 0.8[a,d]
C18:1-ceramide	7.6 ± 0.3	10.8 ± 1.1	25.5 ± 2.6[a]	22.4 ± 0.8[a,b]
C20-ceramide	5.2 ± 0.7	9.1 ± 0.5	21.4 ± 1.8[a]	17.6 ± 1.2[a,b]
C20:1-ceramide	1.5 ± 0.2	2.3 ± 0.2	5.3 ± 0.6[a]	3.9 ± 0.3[a]
C22-ceramide	51.6 ± 2.7	37.5 ± 3.2	132.7 ± 10.6[a]	100.3 ± 3.0[a,d]
C22:1-ceramide	18.7 ± 1.7	16.1 ± 1.9	49.6 ± 4.5[a]	34.6 ± 1.5[a,d]
C24-ceramide	161.9 ± 9.1	97.7 ± 5.1	252.6 ± 22.4[a]	175.2 ± 8.9[d]
C24:1-ceramide	199.3 ± 9.4	110.0 ± 8.6[a]	305.4 ± 28.6[a]	196.7 ± 9.0[d]
C26-ceramide	15.8 ± 3.6	10.6 ± 0.8	13.9 ± 1.3	11.0 ± 1.0
C26:1-ceramide	33.4 ± 3.2	20.1 ± 1.8[a]	33.5 ± 2.3	23.0 ± 2.3[a,c]

SCC17B cells were treated with PDT (20 nM Pc4+200 mJ/cm^2), 4HPR (2.5 μM) or the combination, incubated for 10 h, collected, and processed for MS. Ceramide levels were calculated as pmoles/mg protein and are shown as the average ± SEM (n=3-4). Significant differences are shown between: [a], treatment and untreated control; [b], combination and 4HPR; [c], combination and PDT; [d], combination and both individual treatments. Con, untreated control (Taken from Int. J. Oncol. 46, 2003-10, 2015).

PDT+4HPR-enhanced Bax associated with mitochondria and cyt c redistribution is inhibited by FB.

The mitochondrial apoptosis pathway, including Bax translocation to mitochondria and cyt c redistribution, is induced by PDT and 4HPR [16, 18, 19]. The question is whether the mitochondrial apoptosis pathway is affected by combining PDT with 4HPR, and whether the process is ceramide synthase-dependent. Using quantitative confocal microscopy, we found

that Bax associated with mitochondria and cyt c redistribution were induced after PDT and 4HPR (Figs. 3.8 and 3.9). PDT+4HPR enhanced Bax associated with mitochondria and cyt c redistribution, and FB inhibited both processes.

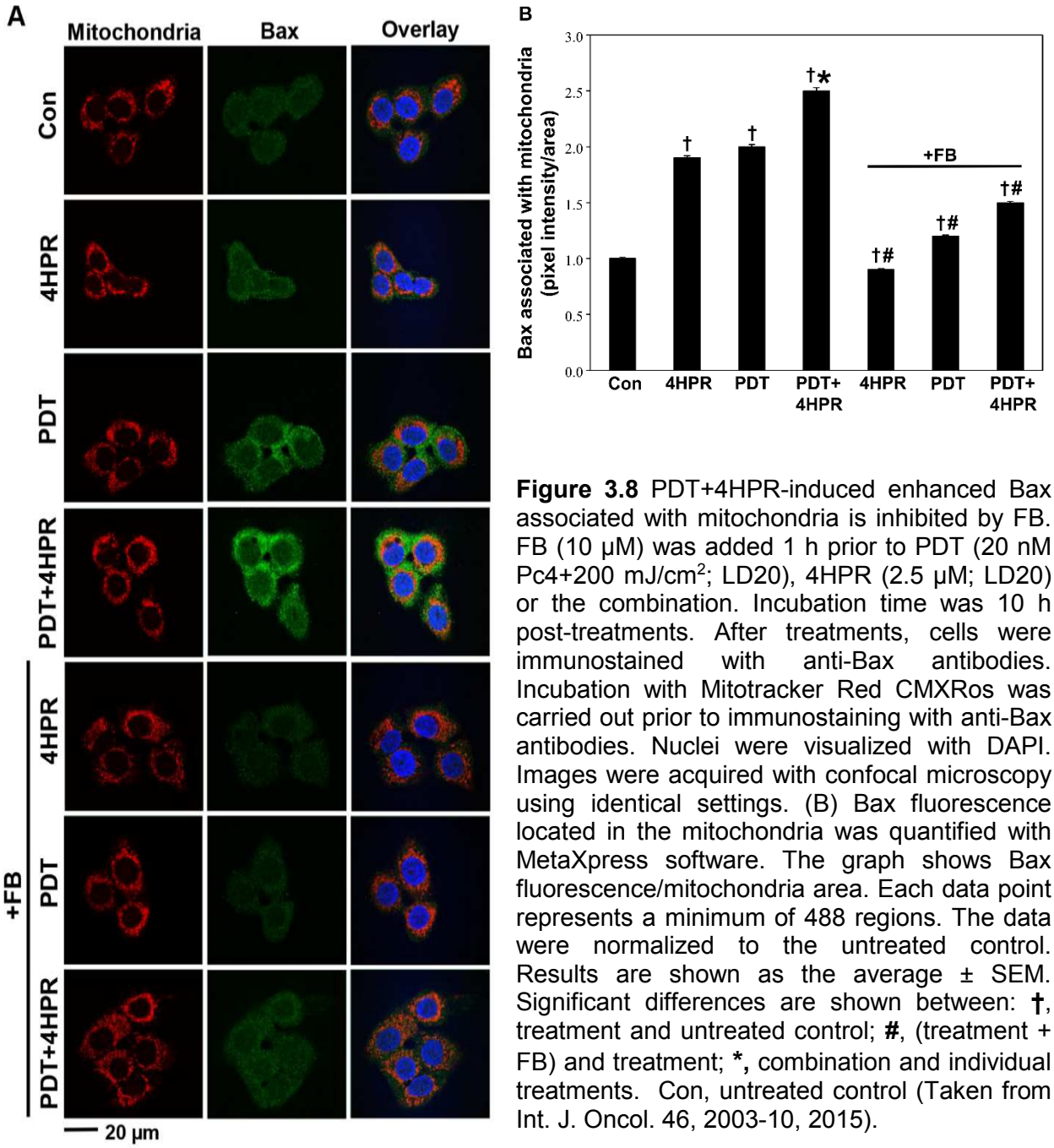

Figure 3.8 PDT+4HPR-induced enhanced Bax associated with mitochondria is inhibited by FB. FB (10 µM) was added 1 h prior to PDT (20 nM Pc4+200 mJ/cm^2; LD20), 4HPR (2.5 µM; LD20) or the combination. Incubation time was 10 h post-treatments. After treatments, cells were immunostained with anti-Bax antibodies. Incubation with Mitotracker Red CMXRos was carried out prior to immunostaining with anti-Bax antibodies. Nuclei were visualized with DAPI. Images were acquired with confocal microscopy using identical settings. (B) Bax fluorescence located in the mitochondria was quantified with MetaXpress software. The graph shows Bax fluorescence/mitochondria area. Each data point represents a minimum of 488 regions. The data were normalized to the untreated control. Results are shown as the average ± SEM. Significant differences are shown between: **†**, treatment and untreated control; **#**, (treatment + FB) and treatment; ***,** combination and individual treatments. Con, untreated control (Taken from Int. J. Oncol. 46, 2003-10, 2015).

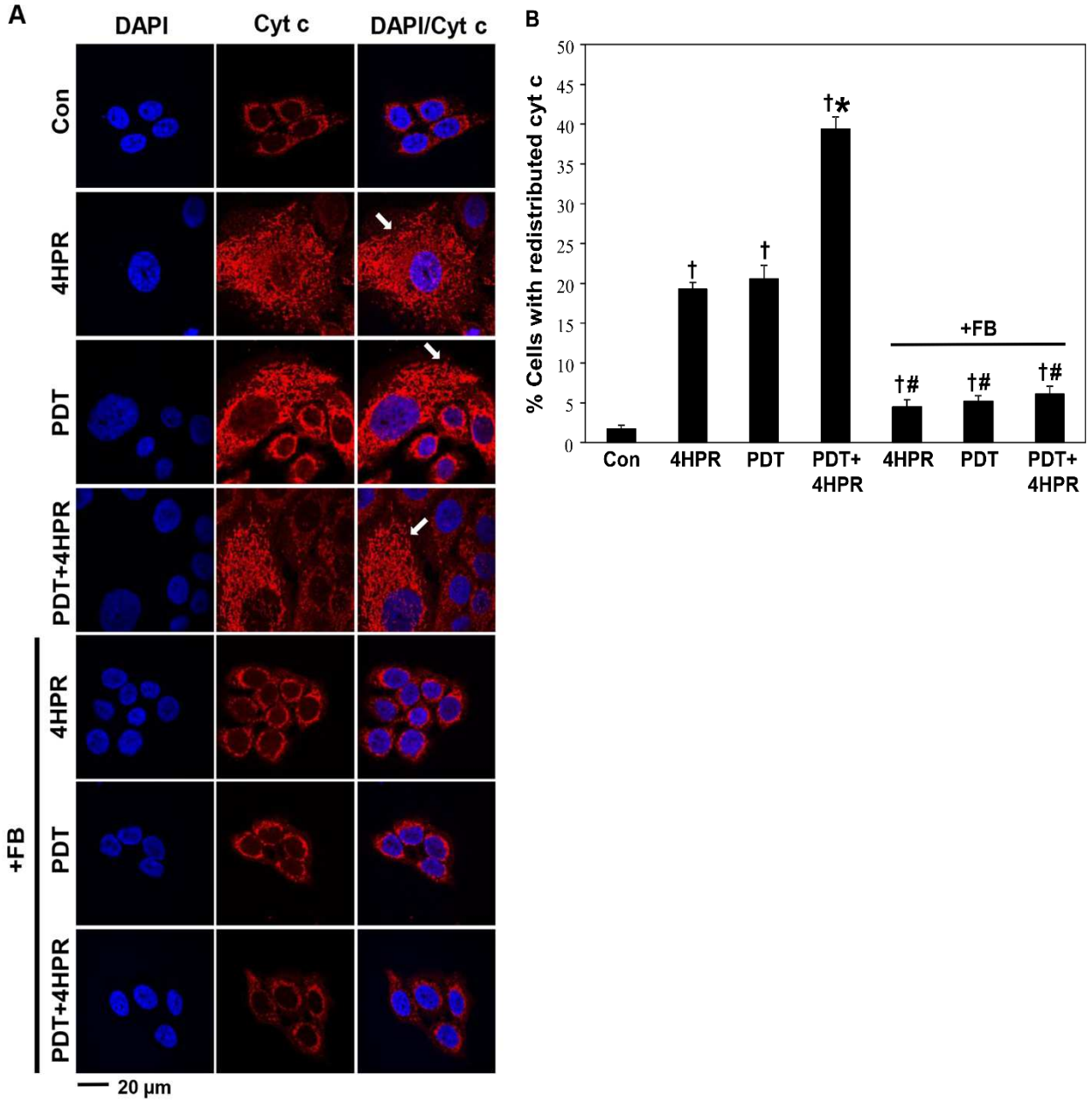

Figure 3.9 PDT+4HPR-induced enhanced cytochrome c redistribution is inhibited by FB. FB (10 µM) was added 1 h prior to PDT (20 nM Pc4+200 mJ/cm^2; LD20), 4HPR (2.5 µM; LD20) or the combination. Incubation time was 10 h post-treatments. After treatments, cells were immunostained with anti-cyt c antibodies. Nuclei were visualized with DAPI. Images were acquired with confocal microscopy using identical settings. Arrow (=>) indicates cyt c redistribution. (B) To calculate percentages of cells with redistributed cyt c, at least 100 cells were scored for every samples. Each bar indicates an average ± SEM from 3-4 samples. Significant differences are shown between: **†**, treatment and untreated control; **#**, (treatment + FB) and treatment; ***,** combination and individual treatments. Con, untreated control (Taken from Int. J. Oncol. 46, 2003-10, 2015).

Enhanced caspase-3 activation induced by PDT+4HPR is inhibited by FB

The effect of combining PDT with 4HPR on caspase-3 activation was determined using DEVDase assay. PDT+4HPR led to enhanced caspase-3 activation at 24 h post-treatments. FB led to inhibition of caspase-3 activation after all the treatments (Figure 3.10). Taken together, data indicates that CERS is involved in enhanced caspase-3 activation after PDT+4HPR.

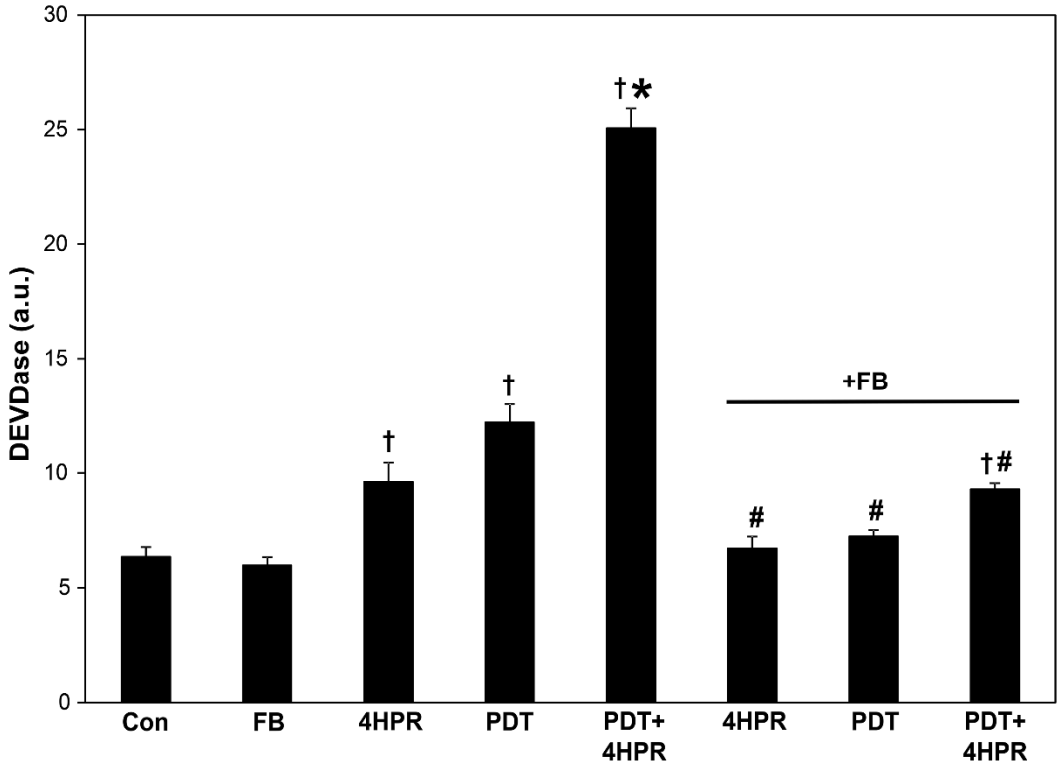

Figure 3.10 PDT+4HPR enhanced FB-sensitive caspase-3 activation. FB (10 μM) was added 1 h prior to PDT (250 nM Pc4 + 200 mJ/cm^2), 4HPR (5 μM) or the combination. Twenty-four h after treatments, cells were collected and processed for DEVDase assay. The data are shown as the average ± SEM (n=3-9 samples). Significant differences are shown between: **†**, treatment and untreated control; **#**, (treatment + FB) and treatment; ***,** combination and individual treatments. Con, control.

Conclusion:

The data suggests that enhanced killing of SCC17B cells after PDT+4HPR depends on ceramide synthase, caspase activation and Bcl2. Combining PDT with 4HPR led to enhanced ER ceramide/dihydroceramide accumulation, Bax associated with mitochondria and cytochrome c redistribution, which were inhibited by FB. PDT+4HPR-induced enhanced C16-dihydroceramide levels but led to attenuation of PDT-induced increase in total and individual ceramide levels. Taken together, these results show that combining PDT with 4HPR enhances cell killing via the *de novo* SL biosynthesis and mitochondrial apoptotic pathway.

3.3 PDT+LCL29 data:

Enhanced cell killing after PDT+LCL29 is FB- and zVAD-sensitive

The clonogenic assay was employed to test whether combining PDT with LCL29 improves PDT efficacy. Each treatment was used at LD20, as determined in dose-response studies (not shown). As depicted in Figure 3.11, combining PDT with LCL29 led to a significant increase in cell killing. To determine whether apoptosis and ceramide synthase are necessary for enhanced cell killing after PDT+LCL29, we used zVAD and FB. The inhibitors alone were non-toxic (LD < 5). As shown in Figure 3.11, FB and zVAD rescued cells from death not only after PDT and LCL29 alone, but also after PDT+LCL29. ABT did not have an effect on PDT+LCL29-induced enhanced cell killing. The data suggest that enhanced cell killing after PDT+LCL29 is mediated by ceramide synthase and caspases.

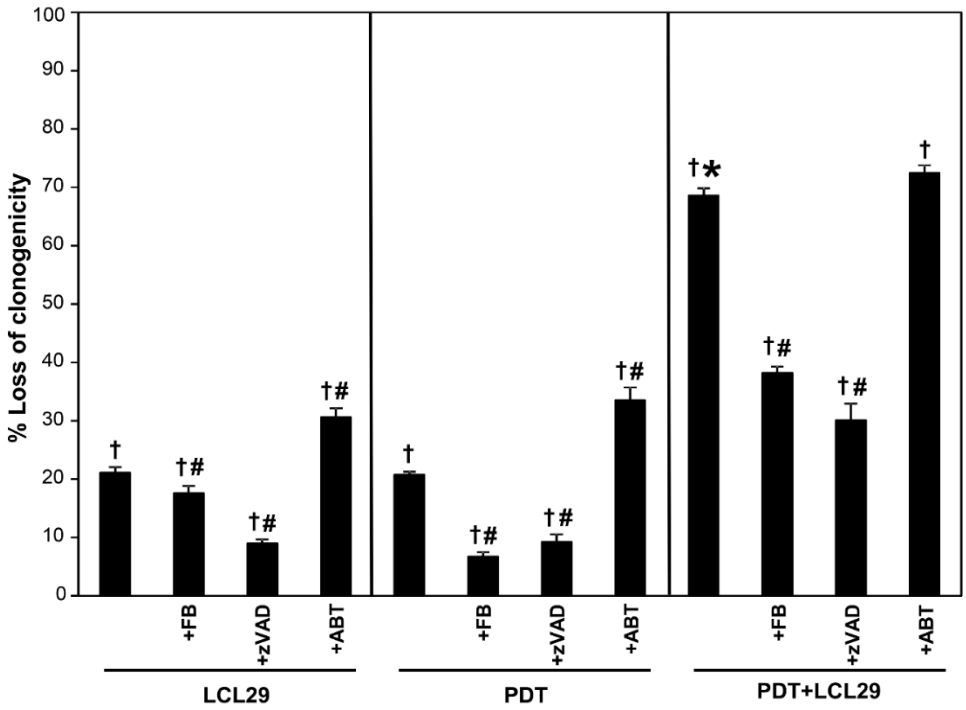

Figure 3.11 Combining PDT with LCL29 enhances loss of clonogenicity in SCC17B cells. The clonogenic potential of PDT±LCL29-treated cells is rescued in the presence of FB and zVAD. FB, zVAD (10 μM each) and ABT (0.1 μM) were added 1 h prior to PDT (20 nM Pc4+200 mJ/cm^2), LCL29 (1 μM) or the combination. Colonies were stained with crystal violet (0.1%) and counted 14 days after treatments. The data are shown as the average ± SEM (n = 3-18 samples). Significant differences are shown between: **†**, treatment and untreated control; **#**, (treatment + inhibitor) and treatment; ***,** combination and individual treatments.

PDT+LCL29 enhances FB-sensitive ceramide/dihydroceramide accumulation in the mitochondria

The biological effects of sphingolipids depend on subcellular site of their generation [49]. Although it has been shown that LCL29 accumulates in mitochondria, it is not known whether mitochondrial ceramide accumulation is induced after LCL29 alone or in combination with PDT. Using the anti-ceramide/dihydroceramide antibody and the mitochondrial marker Mitotracker for quantitative confocal microscopy, we found that PDT and LCL29 alone did induce mitochondrial ceramide/dihydroceramide accumulation (Fig. 3.12). Notably, the effect was enhanced after PDT+LCL29. FB inhibited mitochondrial ceramide/dihydroceramide accumulation after PDT alone or in combination, not after LCL29. Overall, the results suggest ceramide synthase-dependent enhanced mitochondrial ceramide/dihydroceramide accumulation after PDT+LCL29.

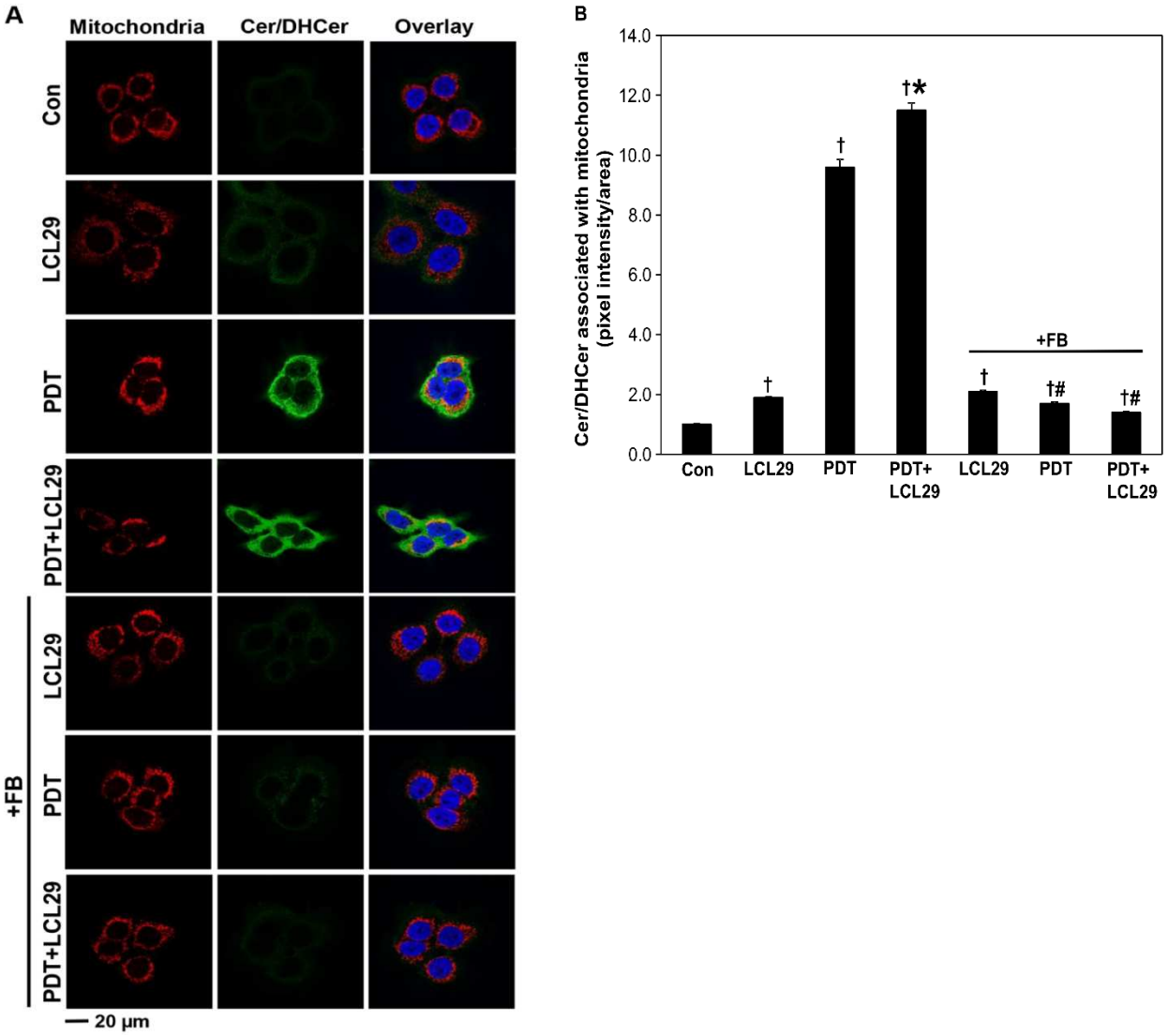

Figure 3.12 PDT+LCL29 enhanced FB-sensitive ceramide/dihydroceramide accumulation in the mitochondria. Cells were treated with FB (10 µM) 1 h prior to PDT (20 nM Pc4+200 mJ/cm^2; LD20), LCL29 (1 µM; LD20) or the combination, and incubated for 10 h. Incubation with Mitotracker Red CMXRos was carried out prior to immunostaining with anti-ceramide/dihydroceramide antibodies. Nuclei were visualized with DAPI. All images were acquired by confocal microscopy with identical settings. MetaXpress software was used to quantify ceramide/dihydroceramide fluorescence located in the mitochondria. Data are shown as the average ± SEM. The graph depicts ceramide/dihydroceramide fluorescence (pixel intensity)/mitochondrial area. Results were normalized to the untreated control. A minimum of 195 regions were measured for each data point. Significant differences are shown between: **†**, treatment and untreated control; **#**, (treatment + FB) and treatment. Con, control Cer, Ceramide; DHCer, Dihydroceramide (Taken from J. Photochem. Photobiol., B 143, 163-8, 2015).

PDT+LCL29 effect on total ceramides

Mass spectrometry data revealed that cellular levels of total ceramides were increased after PDT (Fig. 3.13). LCL29 did not induce any significant cellular ceramide accumulation. Combining PDT with LCL29 did not raise cellular ceramide levels beyond PDT-induced increases in ceramide. The apparent discrepancy between mass spectrometry and confocal microscopy findings for LCL29 alone and the combination argues for measuring ceramide accumulation not only in whole cells but also at a subcellular level. This is important because the subcellular sites of ceramide accumulation affect the specificity of biological effects of this hydrophobic sphingolipid [49].

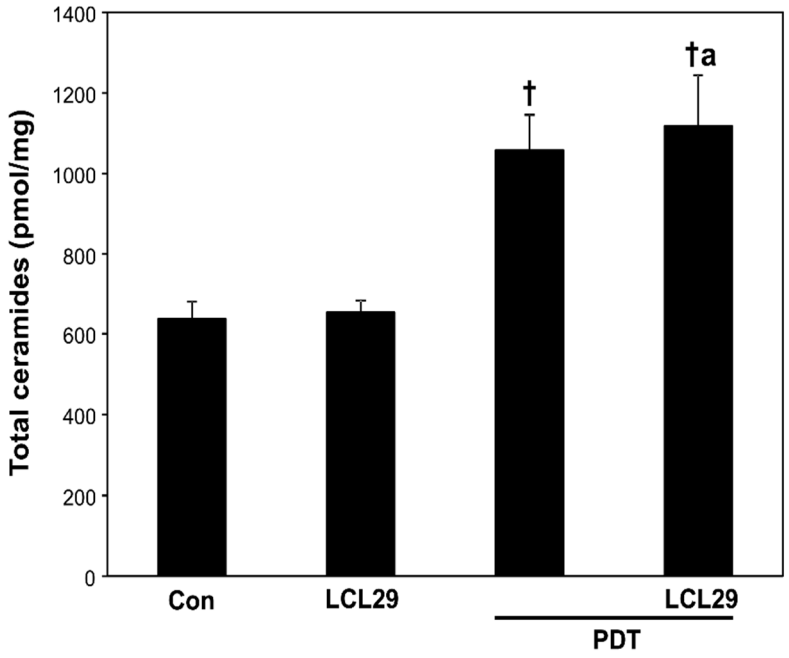

Figure 3.13 Effect of PDT±LCL29 on total ceramide levels. Cells were treated with PDT (20 nM Pc4 + 200 mJ/cm^2; LD20), LCL29 (1 μM; LD20) or the combination, incubated for 10 h, collected, and processed for MS. The levels of sphingolipids were calculated as pmoles/mg protein and are shown as the average ± SEM (n=3-4). Significant differences are shown between: †, treatment and untreated control; [a], (PDT+LCL29) and LCL29. Con, untreated control (Taken from J. Photochem. Photobiol., B 143, 163-8, 2015).

PDT+LCL29-induced enhanced cyt c redistribution is inhibited by FB

The mitochondrial apoptosis pathway, including cyt c redistribution, is induced by PDT and LCL29 [22, 45]. The question is whether cyt c redistribution is regulated by combining PDT with LCL29 and whether the process is ceramide synthase-dependent. Using quantitative confocal microscopy, we found that cells treated with PDT or PDT+LCL29 showed an enhanced redistribution of cyt c staining (Fig. 3.14). In the presence of FB, cyt c redistribution was prevented after PDT alone or in combination, not after LCL29 itself. The data indicate ceramide synthase-dependent cyt c redistribution post-PDT with or without LCL29.

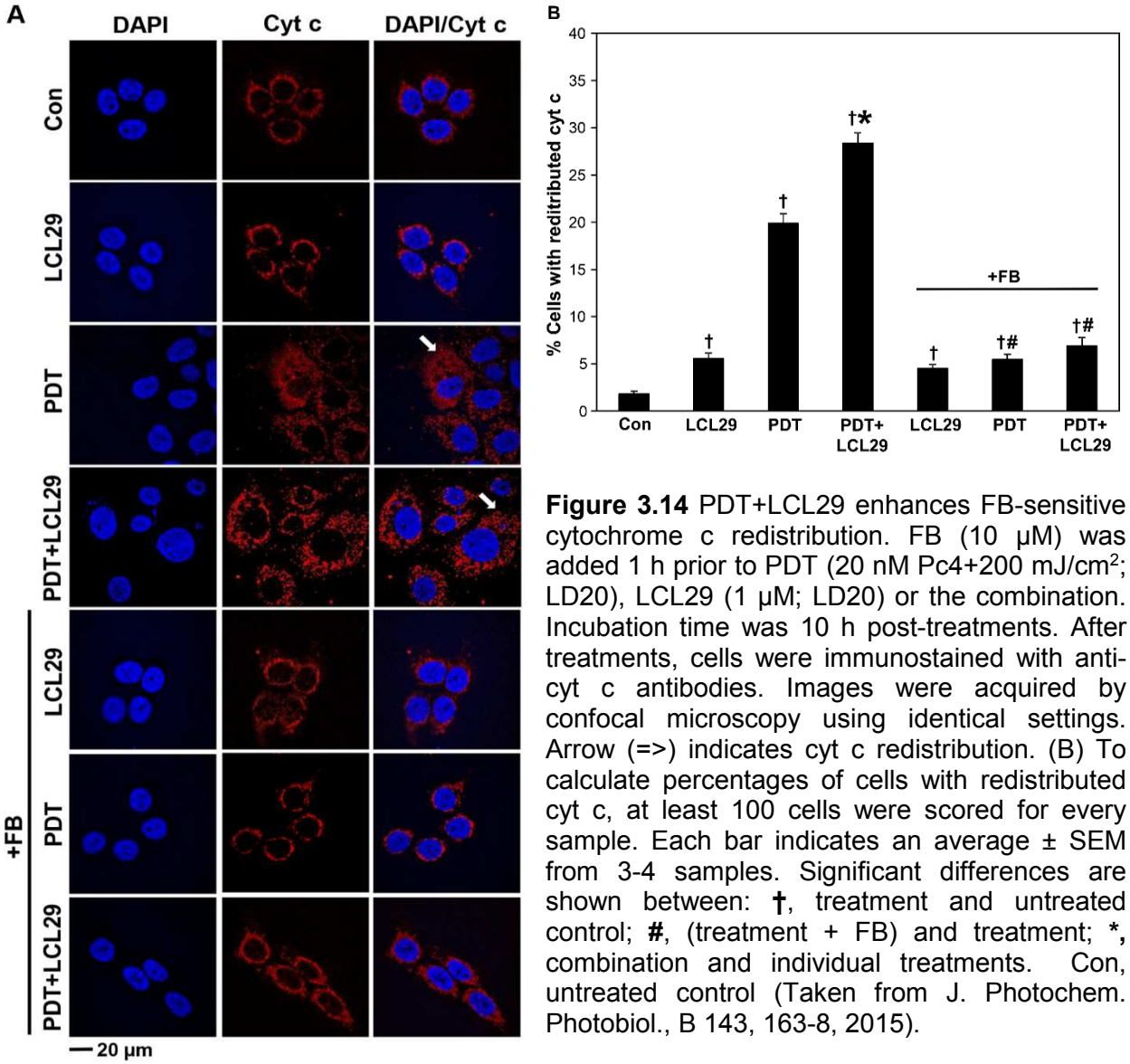

Figure 3.14 PDT+LCL29 enhances FB-sensitive cytochrome c redistribution. FB (10 µM) was added 1 h prior to PDT (20 nM Pc4+200 mJ/cm^2; LD20), LCL29 (1 µM; LD20) or the combination. Incubation time was 10 h post-treatments. After treatments, cells were immunostained with anti-cyt c antibodies. Images were acquired by confocal microscopy using identical settings. Arrow (=>) indicates cyt c redistribution. (B) To calculate percentages of cells with redistributed cyt c, at least 100 cells were scored for every sample. Each bar indicates an average ± SEM from 3-4 samples. Significant differences are shown between: **†**, treatment and untreated control; **#**, (treatment + FB) and treatment; ***,** combination and individual treatments. Con, untreated control (Taken from J. Photochem. Photobiol., B 143, 163-8, 2015).

FB inhibits enhanced caspase-3 activation induced by PDT+LCL29

The effect of treatments on caspase-3 activation was tested using DEVDase assay. As shown in figure 3.15, enhanced caspase-3 activation was observed with PDT+LCL29. Caspase-3 activation after PDT and PDT+LCL29 were inhibited by FB. This shows that CERS is involved in enhanced caspase-3 activation after PDT+LCL29.

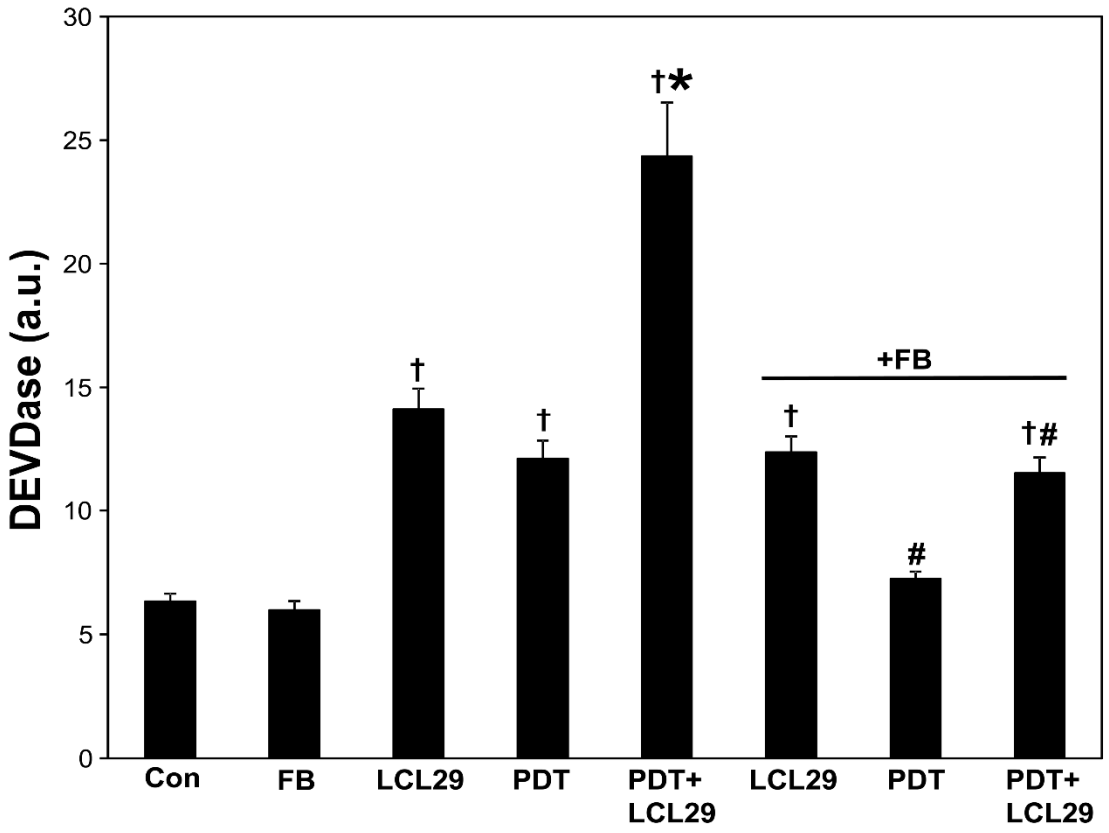

Figure 3.15 PDT+LCL29 enhanced FB-sensitive caspase-3 activation. FB (10 μM) was added 1 h prior to PDT (250 nM Pc4 + 200 mJ/cm^2), LCL29 (5 μM) or the combination. Twenty-four h after treatments, cells were collected and processed for DEVDase assay. The data are shown as the average ± SEM (n=3-12 samples). Significant differences are shown between: **†**, treatment and untreated control; **#**, (treatment + FB) and treatment; *****, combination and individual treatments. Con, control (Taken from J. Photochem. Photobiol., B 143, 163-8, 2015).

Conclusion:

Combining PDT with LCL29 resulted in enhanced cell killing via ceramide synthase and caspases. Enhanced, FB-sensitive mitochondrial ceramide/dihydroceramide accumulation correlates with enhanced mitochondrial apoptosis and cell killing after combining PDT and LCL29. FB sensitivity of the mitochondrial ceramide/dihydroceramide accumulation, cyt c redistribution and caspase-3 were shown for PDT alone or in combination, but not for LCL29. The data further support the role for ceramide synthase-dependent mitochondrial ceramide/dihydroceramide accumulation and apoptosis in advancing cytotoxicity of PDT by combination with LCL29.

CHAPTER 4: SUMMARY AND FUTURE DIRECTIONS

SUMMARY

In summary, the data indicate that PDT-induced cell killing was mediated by ceramide synthase-dependent ceramide/dihydroceramide accumulation and mitochondrial apoptosis. These findings highlight the role of modulating *de novo* sphingolipid biosynthesis in cell killing after PDT. The data also suggest that drugs like LCL29 and 4HPR increase the sensitivity of SCC17B human head and neck squamous cell carcinoma cells to PDT via *de novo* sphingolipid biosynthesis and mitochondrial apoptotic pathway. Figure 4.1 below summarizes the proposed model of cell killing based on the findings of this study.

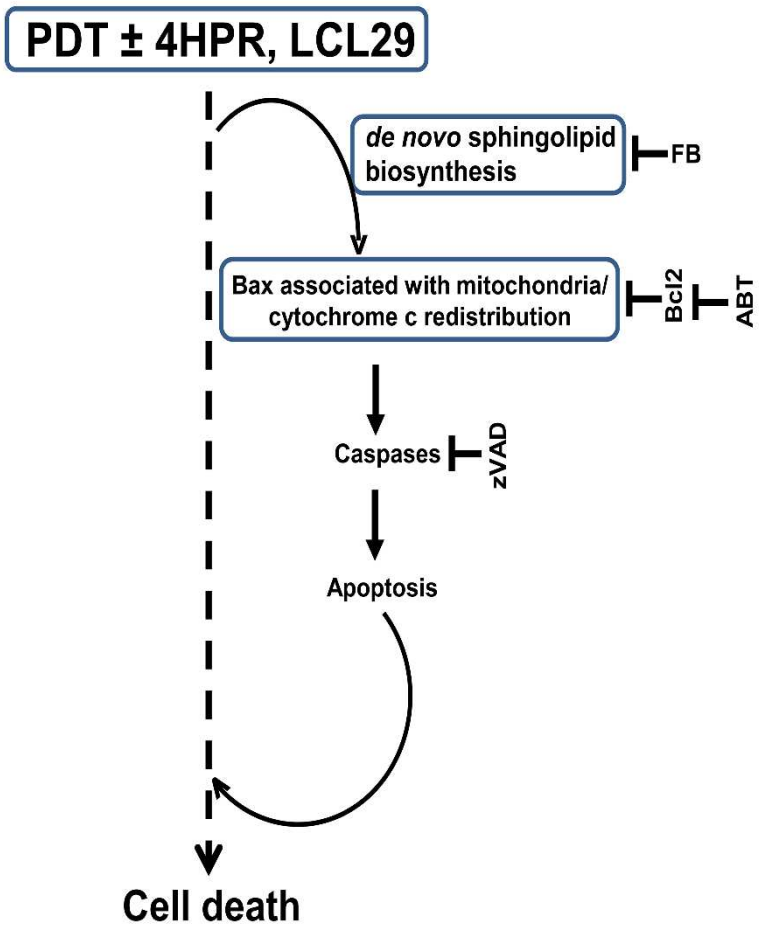

Figure 4.1 Model of cell killing

FUTURE DIRECTIONS

This study has shown that *de novo* generated ceramide/dihydroceramide accumulation and mitochondrial apoptosis play a key role in cell killing after PDT, PDT+4HPR and PDT+LCL29. These results highlight the role of modulating ceramide/dihydroceramide accumulation to improve cell killing after PDT and combinations. But, the mechanism through which ceramide/dihydroceramide accumulation is involved in mitochondrial apoptosis and cell killing is still unknown. Studies have shown that radiation induces formation of ceramide-rich macrodomains in outer mitochondrial membrane. Formation of mitochondrial ceramide-rich macrodomains facilitated cytochrome c release leading to apoptotic cell death [44]. Future directions involve testing the presence of mitochondrial ceramide-rich macrodomains after PDT and how these are involved in cell killing. This opens a new frontier for anti-cancer treatments that modulate the formation of these mitochondrial ceramide-rich macrodomains to induce apoptosis.

Apart from this, pharmacological inhibitors are not always the best tools to test the role of different targets in cell killing. Further studies also include using molecular biology tools like siRNA to knockdown different targets like ceramide synthase, Bcl2 and caspases to validate their role in cell killing after Pc4PDT and combinations. From the study, Bcl2 has been shown to be involved in cell killing after PDT.

APPENDIX

Portions of the text and associated figures in chapters 2 and 3 were taken from prior publications [50-52] (Photochem. Photobiol. 13, 1621-27, 2014**;** J. Photochem. Photobiol., B 143, 163-8, 2015**;** Int. J. Oncol. 46, 2003-10, 2015).

REFERENCES

[1] M. Triesscheijn, P. Baas, J.H. Schellens, F.A. Stewart, Photodynamic therapy in oncology, The oncologist, 11 (2006) 1034-1044.

[2] R.R. Allison, G.H. Downie, R. Cuenca, X.H. Hu, C.J. Childs, C.H. Sibata, Photosensitizers in clinical PDT, Photodiagnosis and photodynamic therapy, 1 (2004) 27-42.

[3] M.H. Schmidt, D.M. Bajic, K.W. Reichert, 2nd, T.S. Martin, G.A. Meyer, H.T. Whelan, Light-emitting diodes as a light source for intraoperative photodynamic therapy, Neurosurgery, 38 (1996) 552-556; discussion 556-557.

[4] Z. Huang, A review of progress in clinical photodynamic therapy, Technol Cancer Res Treat, 4 (2005) 283-293.

[5] D.E. Dolmans, D. Fukumura, R.K. Jain, Photodynamic therapy for cancer, Nature reviews. Cancer, 3 (2003) 380-387.

[6] R.R. Allison, K. Moghissi, Photodynamic Therapy (PDT): PDT Mechanisms, Clinical endoscopy, 46 (2013) 24-29.

[7] S.M. Chiu, L.Y. Xue, K. Azizuddin, N.L. Oleinick, Photodynamic therapy-induced death of HCT 116 cells: Apoptosis with or without Bax expression, Apoptosis : an international journal on programmed cell death, 10 (2005) 1357-1368.

[8] S. Gupta, N. Ahmad, H. Mukhtar, Involvement of nitric oxide during phthalocyanine (Pc4) photodynamic therapy-mediated apoptosis, Cancer research, 58 (1998) 1785-1788.

[9] J. Usuda, S.M. Chiu, K. Azizuddin, L.Y. Xue, M. Lam, A.L. Nieminen, N.L. Oleinick, Promotion of photodynamic therapy-induced apoptosis by the mitochondrial protein Smac/DIABLO: dependence on Bax, Photochemistry and photobiology, 76 (2002) 217-223.

[10] B. Wispriyono, E. Schmelz, H. Pelayo, K. Hanada, D. Separovic, A role for the de novo sphingolipids in apoptosis of photosensitized cells, Experimental cell research, 279 (2002) 153-165.

[11] D. Separovic, P. Breen, N. Joseph, J. Bielawski, J.S. Pierce, V.A.N.B. E, T.I. Gudz, Ceramide synthase 6 knockdown suppresses apoptosis after photodynamic therapy in human head and neck squamous carcinoma cells, Anticancer research, 32 (2012) 753-760.

[12] D. Separovic, P. Breen, N. Joseph, J. Bielawski, J.S. Pierce, V.A.N.B. E, T.I. Gudz, siRNA-mediated down-regulation of ceramide synthase 1 leads to apoptotic resistance in human head and neck squamous carcinoma cells after photodynamic therapy, Anticancer research, 32 (2012) 2479-2485.

[13] L.Y. Xue, S.M. Chiu, N.L. Oleinick, Photochemical destruction of the Bcl-2 oncoprotein during photodynamic therapy with the phthalocyanine photosensitizer Pc 4, Oncogene, 20 (2001) 3420-3427.

[14] J. Usuda, K. Azizuddin, S.M. Chiu, N.L. Oleinick, Association between the photodynamic loss of Bcl-2 and the sensitivity to apoptosis caused by phthalocyanine photodynamic therapy, Photochemistry and photobiology, 78 (2003) 1-8.

[15] M. Srivastava, N. Ahmad, S. Gupta, H. Mukhtar, Involvement of Bcl-2 and Bax in photodynamic therapy-mediated apoptosis. Antisense Bcl-2 oligonucleotide sensitizes RIF 1 cells to photodynamic therapy apoptosis, The Journal of biological chemistry, 276 (2001) 15481-15488.

[16] S.M. Chiu, L.Y. Xue, J. Usuda, K. Azizuddin, N.L. Oleinick, Bax is essential for mitochondrion-mediated apoptosis but not for cell death caused by photodynamic therapy, British journal of cancer, 89 (2003) 1590-1597.

[17] M. Lam, N.L. Oleinick, A.L. Nieminen, Photodynamic therapy-induced apoptosis in epidermoid carcinoma cells. Reactive oxygen species and mitochondrial inner membrane permeabilization, The Journal of biological chemistry, 276 (2001) 47379-47386.

[18] M. Tiwari, A. Kumar, R.A. Sinha, A. Shrivastava, A.K. Balapure, R. Sharma, V.K. Bajpai, K. Mitra, S. Babu, M.M. Godbole, Mechanism of 4-HPR-induced apoptosis in glioma cells:

evidences suggesting role of mitochondrial-mediated pathway and endoplasmic reticulum stress, Carcinogenesis, 27 (2006) 2047-2058.

[19] E. Ulukaya, G. Pirianov, M.A. Kurt, E.J. Wood, H. Mehmet, Fenretinide induces cytochrome c release, caspase 9 activation and apoptosis in the absence of mitochondrial membrane depolarisation, Cell death and differentiation, 10 (2003) 856-859.

[20] Z.M. Szulc, J. Bielawski, H. Gracz, M. Gustilo, N. Mayroo, Y.A. Hannun, L.M. Obeid, A. Bielawska, Tailoring structure-function and targeting properties of ceramides by site-specific cationization, Bioorganic & medicinal chemistry, 14 (2006) 7083-7104.

[21] J.S. Modica-Napolitano, J.R. Aprille, Delocalized lipophilic cations selectively target the mitochondria of carcinoma cells, Advanced drug delivery reviews, 49 (2001) 63-70.

[22] Q. Hou, J. Jin, H. Zhou, S.A. Novgorodov, A. Bielawska, Z.M. Szulc, Y.A. Hannun, L.M. Obeid, Y.T. Hsu, Mitochondrially targeted ceramides preferentially promote autophagy, retard cell growth, and induce apoptosis, Journal of lipid research, 52 (2011) 278-288.

[23] D. Separovic, J. Bielawski, J.S. Pierce, S. Merchant, A.L. Tarca, G. Bhatti, B. Ogretmen, M. Korbelik, Enhanced tumor cures after Foscan photodynamic therapy combined with the ceramide analog LCL29. Evidence from mouse squamous cell carcinomas for sphingolipids as biomarkers of treatment response, International journal of oncology, 38 (2011) 521-527.

[24] D. Separovic, J. Bielawski, J.S. Pierce, S. Merchant, A.L. Tarca, B. Ogretmen, M. Korbelik, Increased tumour dihydroceramide production after Photofrin-PDT alone and improved tumour response after the combination with the ceramide analogue LCL29. Evidence from mouse squamous cell carcinomas, British journal of cancer, 100 (2009) 626-632.

[25] U. Veronesi, L. Mariani, A. Decensi, F. Formelli, T. Camerini, R. Miceli, M.G. Di Mauro, A. Costa, E. Marubini, M.B. Sporn, G. De Palo, Fifteen-year results of a randomized phase III trial of fenretinide to prevent second breast cancer, Annals of oncology : official journal of the European Society for Medical Oncology / ESMO, 17 (2006) 1065-1071.

[26] F. Chiesa, N. Tradati, M. Marazza, N. Rossi, P. Boracchi, L. Mariani, M. Clerici, F. Formelli, L. Barzan, A. Carrassi, et al., Prevention of local relapses and new localisations of oral leukoplakias with the synthetic retinoid fenretinide (4-HPR). Preliminary results, European journal of cancer. Part B, Oral oncology, 28B (1992) 97-102.

[27] N. Oridate, D. Lotan, X.C. Xu, W.K. Hong, R. Lotan, Differential induction of apoptosis by all-trans-retinoic acid and N-(4-hydroxyphenyl)retinamide in human head and neck squamous cell carcinoma cell lines, Clinical cancer research : an official journal of the American Association for Cancer Research, 2 (1996) 855-863.

[28] A. Mariotti, E. Marcora, G. Bunone, A. Costa, U. Veronesi, M.A. Pierotti, G. Della Valle, N-(4-hydroxyphenyl)retinamide: a potent inducer of apoptosis in human neuroblastoma cells, Journal of the National Cancer Institute, 86 (1994) 1245-1247.

[29] M. Cuello, A.O. Coats, I. Darko, S.A. Ettenberg, G.J. Gardner, M.M. Nau, J.R. Liu, M.J. Birrer, S. Lipkowitz, N-(4-hydroxyphenyl) retinamide (4HPR) enhances TRAIL-mediated apoptosis through enhancement of a mitochondrial-dependent amplification loop in ovarian cancer cell lines, Cell death and differentiation, 11 (2004) 527-541.

[30] R.L. Scher, W. Saito, R.K. Dodge, W.J. Richtsmeier, R.L. Fine, Fenretinide-induced apoptosis of human head and neck squamous carcinoma cell lines, Otolaryngology--head and neck surgery : official journal of American Academy of Otolaryngology-Head and Neck Surgery, 118 (1998) 464-471.

[31] S. Elmore, Apoptosis: a review of programmed cell death, Toxicologic pathology, 35 (2007) 495-516.

[32] D.M. Finucane, E. Bossy-Wetzel, N.J. Waterhouse, T.G. Cotter, D.R. Green, Bax-induced caspase activation and apoptosis via cytochrome c release from mitochondria is inhibitable by Bcl-xL, The Journal of biological chemistry, 274 (1999) 2225-2233.

[33] M. Garcia-Calvo, E.P. Peterson, B. Leiting, R. Ruel, D.W. Nicholson, N.A. Thornberry, Inhibition of human caspases by peptide-based and macromolecular inhibitors, The Journal of biological chemistry, 273 (1998) 32608-32613.

[34] A.J. Souers, J.D. Leverson, E.R. Boghaert, S.L. Ackler, N.D. Catron, J. Chen, B.D. Dayton, H. Ding, S.H. Enschede, W.J. Fairbrother, D.C. Huang, S.G. Hymowitz, S. Jin, S.L. Khaw, P.J. Kovar, L.T. Lam, J. Lee, H.L. Maecker, K.C. Marsh, K.D. Mason, M.J. Mitten, P.M. Nimmer, A. Oleksijew, C.H. Park, C.M. Park, D.C. Phillips, A.W. Roberts, D. Sampath, J.F. Seymour, M.L. Smith, G.M. Sullivan, S.K. Tahir, C. Tse, M.D. Wendt, Y. Xiao, J.C. Xue, H. Zhang, R.A. Humerickhouse, S.H. Rosenberg, S.W. Elmore, ABT-199, a potent and selective BCL-2 inhibitor, achieves antitumor activity while sparing platelets, Nature medicine, 19 (2013) 202-208.

[35] A.H. Merrill, Jr., De novo sphingolipid biosynthesis: a necessary, but dangerous, pathway, The Journal of biological chemistry, 277 (2002) 25843-25846.

[36] E. Wang, W.P. Norred, C.W. Bacon, R.T. Riley, A.H. Merrill, Jr., Inhibition of sphingolipid biosynthesis by fumonisins. Implications for diseases associated with Fusarium moniliforme, The Journal of biological chemistry, 266 (1991) 14486-14490.

[37] W.I. Wu, V.M. McDonough, J.T. Nickels, Jr., J. Ko, A.S. Fischl, T.R. Vales, A.H. Merrill, Jr., G.M. Carman, Regulation of lipid biosynthesis in Saccharomyces cerevisiae by fumonisin B1, The Journal of biological chemistry, 270 (1995) 13171-13178.

[38] D. Separovic, Z.H. Saad, E.A. Edwin, J. Bielawski, J.S. Pierce, E.V. Buren, A. Bielawska, C16-Ceramide Analog Combined with Pc 4 Photodynamic Therapy Evokes Enhanced Total Ceramide Accumulation, Promotion of DEVDase Activation in the Absence of Apoptosis, and Augmented Overall Cell Killing, Journal of lipids, 2011 (2011) 713867.

[39] M. Kodiha, C.M. Brown, U. Stochaj, Analysis of signaling events by combining high-throughput screening technology with computer-based image analysis, Science signaling, 1 (2008) pl2.

[40] D. Separovic, L. Semaan, A.L. Tarca, M.Y. Awad Maitah, K. Hanada, J. Bielawski, M. Villani, C. Luberto, Suppression of sphingomyelin synthase 1 by small interference RNA is associated with enhanced ceramide production and apoptosis after photodamage, Experimental cell research, 314 (2008) 1860-1868.

[41] V. Dolgachev, M.S. Farooqui, O.I. Kulaeva, M.A. Tainsky, B. Nagy, K. Hanada, D. Separovic, De novo ceramide accumulation due to inhibition of its conversion to complex sphingolipids in apoptotic photosensitized cells, The Journal of biological chemistry, 279 (2004) 23238-23249.

[42] L.Y. Xue, S.M. Chiu, K. Azizuddin, S. Joseph, N.L. Oleinick, Protection by Bcl-2 against apoptotic but not autophagic cell death after photodynamic therapy, Autophagy, 4 (2008) 125-127.

[43] C.E. Senkal, S. Ponnusamy, Y. Manevich, M. Meyers-Needham, S.A. Saddoughi, A. Mukhopadyay, P. Dent, J. Bielawski, B. Ogretmen, Alteration of ceramide synthase 6/C16-ceramide induces activating transcription factor 6-mediated endoplasmic reticulum (ER) stress and apoptosis via perturbation of cellular Ca2+ and ER/Golgi membrane network, The Journal of biological chemistry, 286 (2011) 42446-42458.

[44] H. Lee, J.A. Rotolo, J. Mesicek, T. Penate-Medina, A. Rimner, W.C. Liao, X. Yin, G. Ragupathi, D. Ehleiter, E. Gulbins, D. Zhai, J.C. Reed, A. Haimovitz-Friedman, Z. Fuks, R. Kolesnick, Mitochondrial ceramide-rich macrodomains functionalize Bax upon irradiation, PloS one, 6 (2011) e19783.

[45] S.M. Chiu, N.L. Oleinick, Dissociation of mitochondrial depolarization from cytochrome c release during apoptosis induced by photodynamic therapy, British journal of cancer, 84 (2001) 1099-1106.

[46] L.A. Cowart, Z. Szulc, A. Bielawska, Y.A. Hannun, Structural determinants of sphingolipid recognition by commercially available anti-ceramide antibodies, Journal of lipid research, 43 (2002) 2042-2048.

[47] J.M. Kraveka, L. Li, Z.M. Szulc, J. Bielawski, B. Ogretmen, Y.A. Hannun, L.M. Obeid, A. Bielawska, Involvement of dihydroceramide desaturase in cell cycle progression in human neuroblastoma cells, The Journal of biological chemistry, 282 (2007) 16718-16728.

[48] F. Rehman, P. Shanmugasundaram, M.P. Schrey, Fenretinide stimulates redox-sensitive ceramide production in breast cancer cells: potential role in drug-induced cytotoxicity, British journal of cancer, 91 (2004) 1821-1828.

[49] Y.A. Hannun, L.M. Obeid, Many ceramides, The Journal of biological chemistry, 286 (2011) 27855-27862.

[50] N.B. Boppana, M. Kodiha, U. Stochaj, H.S. Lin, A. Haimovitz-Friedman, A. Bielawska, J. Bielawski, G.W. Divine, J.A. Boyd, M. Korbelik, D. Separovic, Ceramide synthase inhibitor fumonisin B1 inhibits apoptotic cell death in SCC17B human head and neck squamous carcinoma cells after Pc4 photosensitization, Photochemical & photobiological sciences : Official journal of the European Photochemistry Association and the European Society for Photobiology, 13 (2014) 1621-1627.

[51] N.B. Boppana, U. Stochaj, M. Kodiha, A. Bielawska, J. Bielawski, J.S. Pierce, M. Korbelik, D. Separovic, C6-pyridinium ceramide sensitizes SCC17B human head and neck squamous cell carcinoma cells to photodynamic therapy, Journal of photochemistry and photobiology. B, Biology, 143 (2015) 163-168.

[52] N.B. Boppana, U. Stochaj, M. Kodiha, A. Bielawska, J. Bielawski, J.S. Pierce, M. Korbelik, D. Separovic, Enhanced killing of SCC17B human head and neck squamous cell carcinoma cells after photodynamic therapy plus fenretinide via the de novo sphingolipid biosynthesis pathway and apoptosis, International journal of oncology, 46 (2015) 2003-2010.

ABSTRACT

COMBINATION OF PHOTODYNAMIC THERAPY WITH FENRETINIDE AND C6-PYRIDINIUM CERAMIDE ENHANCES KILLING OF SCC17B HUMAN HEAD AND NECK SQUAMOUS CELL CARCINOMA CELLS VIA THE *DE NOVO* SPHINGOLIPID BIOSYNTHESIS AND MITOCHONDRIAL APOPTOSIS

by

NITHIN BHARGAVA BOPPANA

August 2015

Advisor: Dr. Duska Separovic

Major: Pharmaceutical Sciences

Degree: Master of Science

The ceramide generated via the *de novo* sphingolipid biosynthesis has been shown to regulate apoptosis and cell death. The *de novo* sphingolipid biosynthesis includes ceramide synthase (CERS)-dependent acylation of dihydrosphingosine, giving rise to dihydroceramide, which is then converted to ceramide by a desaturase-dependent reaction. The mitochondrial pathway of apoptosis, characterized by induction of Bax associated with mitochondria and cytochrome c release/redistribution. Bcl2, an anti-apoptotic protein blocks apoptosis by inhibiting Bax. Elucidating the role of *de novo* sphingolipid biosynthesis and mitochondrial apoptosis in PDT, PDT+4HPR and PDT+LCL29 could help in improving the effectiveness on these anti-cancer treatments. The objective of this study was to determine the involvement of *de novo* sphingolipid biosynthesis and mitochondrial apoptosis in PDT-induced cell killing and testing whether combining LCL29 and 4HPR with PDT enhances cell killing via *de novo* sphingolipid biosynthesis and mitochondrial apoptosis. Silicon phthalocyanine Pc4 was used as a photosensitizer for PDT and SCC17B human head and neck squamous cell carcinoma cells were used in this study.

Results indicate that ceramide synthase, caspases and Bcl2 were involved in PDT-induced cell killing. PDT-induced ER and mitochondrial ceramide/dihydroceramide accumulation

was inhibited by fumonisin B1 (FB) indicating involvement of ceramide synthase. PDT led to increase in majority of individual ceramides and C16-dihydroceramide. FB inhibited mitochondrial apoptotic events like PDT-induced Bax associated with mitochondria, cytochrome c redistribution and caspase-3 activation. The data suggests that PDT-induced cell killing is mediated by ceramide synthase-dependent ceramide/dihydroceramide accumulation and mitochondrial apoptosis. Combining PDT with 4HPR led to enhanced cell killing via ceramide synthase, caspases and Bcl2. PDT+4HPR enhanced ceramide synthase-dependent ER ceramide/dihydroceramide accumulation. Combining PDT with 4HPR enhances C16-dihydroceramide levels but leads to attenuation of total and individual ceramide levels compared to PDT. PDT+4HPR-induced enhanced FB-sensitive Bax associated with mitochondria and cytochrome c redistribution. These data indicate that combining PDT with 4HPR enhanced cell killing via *de novo* sphingolipid biosynthesis and mitochondrial apoptosis. Combining PDT with LCL29 resulted in enhanced cell killing via ceramide synthase and caspases. PDT+LCL29-induced enhanced ceramide/dihydroceramide accumulation in the mitochondria was inhibited by FB. PDT+LCL29 enhanced cytochrome c redistribution and caspase-3 activation were inhibited by FB. Taken together, this study has shown that *de novo* sphingolipid biosynthesis and mitochondrial apoptosis play a key role in killing of SCC17B human head and neck squamous cell carcinoma cells after PDT, PDT+4HPR and PDT+LCL29.

AUTOBIOGRAPHICAL STATEMENT

EDUCATION

2007-2011 Bachelor of Pharmacy, Rajiv Gandhi University of Health Sciences, Karnataka, India

2012-2015 Master of Science in Pharmaceutical Sciences, Wayne State University, MI, USA

HONORS AND AWARDS

Graduate Professional Scholarship (2013-2014), Wayne State University

Thomas C. Rumble Graduate Fellowship (2014-2015), Wayne State University

Best Poster Award for Basic Science, 10th Research forum (2012), EACPHS, Wayne State University

PUBLICATIONS

1. **N.B. Boppana**, M. Kodiha, U. Stochaj, H.S. Lin, A. Haimovitz-Friedman, A. Bielawska, J. Bielawski, G.W. Divine, J.A. Boyd, M. Korbelik, D. Separovic, Ceramide synthase inhibitor fumonisin B1 inhibits apoptotic cell death in SCC17B human head and neck squamous carcinoma cells after Pc4 photosensitization, Photochem Photobiol Sci, 13 (2014) 1621-27.
2. **N.B. Boppana**, U. Stochaj, M. Kodiha, A. Bielawska, J. Bielawski, Jason.S. Pierce, M. Korbelik, D. Separovic, C6-pyridinium ceramide sensitizes SCC17B human head and neck squamous cell carcinoma cells to photodynamic therapy, J. Photochem. Photobiol., B, 143 (2015), 163-8.
3. **N.B. Boppana**, U. Stochaj, M. Kodiha, A. Bielawska, J. Bielawski, Jason.S. Pierce, M. Korbelik, D. Separovic, Enhanced killing of SCC17B human head and neck squamous cell carcinoma cells after photodynamic therapy plus fenretinide via the de novo sphingolipid biosynthesis pathway and apoptosis, Int. J. Oncol., 46 (2015), 2003-10.